ISTANBUL TECHNICAL UNIVERSITY ★ GRADUATE SCHOOL

DETECTION OF LOCAL STRUCTURAL DISTORTIONS IN SKIN DUE TO SKIN CANCER BY RAMAN SPECTROSCOPY AND MACHINE LEARNING

M.Sc. THESIS

Muhammet Melih GÜLER

Department of Computer Sciences

Computer Sciences Programme

MAY 2024

ISTANBUL TECHNICAL UNIVERSITY ★ GRADUATE SCHOOL

DETECTION OF LOCAL STRUCTURAL DISTORTIONS IN SKIN DUE TO SKIN CANCER BY RAMAN SPECTROS COPY AND MACHINE LEARNING

M.Sc. THESIS

Muhammet Melih GÜLER
(704211018)

Department of Computer Sciences

Computer Sciences Programme

Thesis Advisor: Asst. Prof. Dr. Onur KURT

MAY 2024

ISTANBUL TEKNİK ÜNİVERSİTESİ ★ LİSANSÜSTÜ EĞİTİM ENSTİTÜSÜ

CİLT KANSERİNE BAĞLI CİLTTEKİ YEREL YAPISAL BOZULMALARIN RAMAN SPEKTROSKOPİSİ VE MAKİNE ÖĞRENMESİ İLE TESPİTİ

YÜKSEK LİSANS TEZİ

Muhammet Melih GÜLER
(704211018)

Bilgisayar Bilimleri Anabilim Dalı

Bilgisayar Bilimleri Programı

Tez Danışmanı: Dr. Öğr. Üyesi Onur KURT

MAYIS 2024

Muhammet Melih GÜLER, a **M.Sc.** student of ITU Graduate School student ID 704211018, successfully defended the thesis entitled “DETECTION OF LOCAL STRUCTURAL DISTORTIONS IN SKIN DUE TO SKIN CANCER BY RAMAN SPECTROSCOPY AND MACHINE LEARNING”, which he prepared after fulfilling the requirements specified in the associated legislations, before the jury whose signatures are below.

Thesis Advisor : **Asst. Prof. Dr. Onur KURT**
İstanbul Technical University

Jury Members : **Asst. Prof. Dr. Onur KURT**
İstanbul Techincal University

Assoc. Prof. Dr. Serkan TÜRKELİ
Marmara University

Assoc. Prof. Dr. Mehmet Nuri AKINCI
Istanbul Technical University

Date of Submission : 12 June 2024
Date of Defense : 31 May 2024

To my lovely wife,

FOREWORD

I would like to express my sincere gratitude to my supervisor Asst. Prof. Dr. Onur KURT. With his encouragement, efforts, invaluable guidance and support, I have been a fortunate in this study.

I dedicate this thesis to my pure-hearted and lovely wife. Her unlimited support and believe, this study became much easier and possible.

May 2024

Muhammet Melih GÜLER
(Software Engineer)

TABLE OF CONTENTS

Page

ABBREVIATIONS

AI	: Artificial Intelligence
ANN	: Artificial Neural Networks
AUC	: Area Under Curve
BCC	**:** Basal Cell Carcinoma
CART	: Classification and Regression Tree
CNN	: Convolutional Neural Networks
DT	**:** Decision Tree
HRUS	: High-Resolution Ultrasound
ITU	**:** Istanbul Technical University
KNN	**:** K-Nearest Neighbors
LDA	: Linear Discriminant Analysis
LR	**:** Logistic Regression
ML	**:** Machine Learning
MLP	: Multilayer Perceptron
NIR	**:** Near-Infrared
NMF	: Nonnegative Matrix Factorization
NPV	: Negative Predictive Value
PCA	: Principal Component Analysis
PPV	: Positive Predictive Value
RBF	: Radial basis function
RCM	: Reflectance Confocal Microscopy
RF	**:** Random Forest
ROC	**:** Receiver Operating Characteristic
SVC	: Support Vector Classification
SVM	: Support Vector Machine
UBM	: Ultrasound Biomicroscopy

LIST OF TABLES

Page

LIST OF FIGURES

Page

DETECTION OF LOCAL STRUCTURAL DISTORTIONS IN SKIN DUE TO SKIN CANCER BY RAMAN SPECTROSCOPY AND MACHINE LEARNING

SUMMARY

Recently, a significant portion of the global population is grappling with skin cancer, which stands as a widespread and potentially lethal ailment. Analysis of epidemiological data reveals a troubling uptick in skin cancer instances worldwide, emphasizing the critical need for ongoing monitoring and preventative actions. Early diagnosis and precise detection play pivotal roles in effectively managing skin cancer and improving patient outcomes. Timely detection holds immense significance across numerous biomedical applications and diverse medical scenarios, particularly in the realm of addressing skin cancer, where it has the potential to save numerous lives by enabling effective treatment interventions. Among the different types of skin cancer, basal cell carcinoma (BCC) emerges as the most common, frequently manifesting on areas of the skin exposed to sunlight. BCC, characterized by its tendency for local invasion and slow growth, can still potentially metastasize. In the United States, the incidence of BCC stands at 300 cases per 100,000 individuals, with a lifetime risk of 30% due to an annual rise exceeding 10%. Despite its relatively low mortality rate, the condition affects a substantial population, placing significant strain on the healthcare system of the United Kingdom. While conventional procedures for treating BCC are frequently effective, they come with several drawbacks, such as the subjective nature of clinical assessments, the invasive nature of biopsies, and delays in diagnosis. Modern biomedical research, leveraging advanced technologies and analytical methodologies, offers new opportunities for understanding diseases through in-depth biological analysis. Recently, Raman spectroscopy has garnered attention as a potential alternative method for accurately identifying skin malignancies. With the hand of the Raman spectroscopy, the machine learning (ML) methodologies can be integrated for diagnosing the local structural distortions in skin.

This study utilizes Raman spectroscopy and various supervised ML algorithms to identify structural irregularities in tumor-affected tissue compared to normal tissue, aiming to differentiate between BCC subtypes, particularly nodular and infiltrative BCC, with successful tissue discrimination potentially reducing the pathological diagnosis phase, leading to faster recognition rates and decreased mortality.

In this prospective study, approved by the ethics committee of Şisli Hamidiye Etfal Training and Research Hospital in Istanbul, Türkiye, patients diagnosed with BCC underwent total excision by an experienced plastic surgeon after histopathological diagnosis through punch biopsy. Fresh tissue samples of varying sizes are then carefully placed in a container with physiological NaCl solution and transported to Istanbul Technical University (ITU) for Raman spectroscopy investigation. Custom sample holders are created to suppress Raman signals from the aluminum foil-coated microscope slides, making the technique more cost-effective. Raman measurements are conducted on the fresh tissue samples, which are then securely transported back to

the hospital for further examination by skilled pathologists, who identified nodular and infiltrative BCC subgroups. In the next stage, Raman data underwent extensive preprocessing. Initially, cosmic rays were eliminated from the raw Raman data, followed by the removal of fluorescence-induced background in each spectrum. The Savitsky-Golay smoothing method was then applied to refine each detrended spectrum, ensuring the elimination of unnecessary data points and unforeseen noises. Subsequently, normalization was performed on each spectrum to ensure uniformity and comparability across spectral profiles. These preprocessing steps standardized the dataset, reduced noise and volatility, and prepared it for reliable ML analysis. Before constructing classification-based ML models for each Raman spectrum ranging from 400 to 3200 cm^{-1}, the dataset was divided into training and testing subsets, with 80% allocated for training. To mitigate overfitting, 5-fold cross-validation was employed, with validation scores monitored for each instance. Various ML models were utilized in the study, including Random Forest (RF), Decision Tree (DT), k-Nearest Neighbors (KNN), Logistic Regression (LR), Linear Discriminant Analysis (LDA), Multilayer Perceptron (MLP), and Support Vector Machine (SVM). Classification is made for two cases: First, to acquire the discrimination of BCC and noninvasive tissues. Second, to distinguish between nodular BCC and infiltrative BCC tissues.

The results for the BCC and normal tissue discrimination demonstrate that all ML-based classifiers exhibit satisfactory metrics for distinguishing between BCC and normal skin. Among the models, RF and KNN classifiers stand out with the highest accuracy of 98.4%, surpassing others. Conversely, LR and LDA exhibit lower performance, with accuracies of 84.9% and 84.6%, respectively. Also, RF classifiers exhibit comparable performance with the highest macro-averaged accuracy of 98.4% and the maximum area under curve (AUC) score of 99%. Consistently high accuracy and robust performance is observed for both RF and KNN classifiers.

The outputs for the subtypes of BCCs indicate that despite a slight decrease in precision when distinguishing between different subtypes of BCC compared to distinguishing BCC from normal skin, the study's ML classifiers maintained a notably high level of accuracy in discriminating nodular BCC from infiltrative BCC. RF and KNN classifiers demonstrated exemplary performance, achieving accuracies of 89.3% and 90.7%, respectively, outperforming alternative models. Furthermore, both RF and KNN classifiers exhibited sensitivity, specificity, positive predictive value (PPV), negative predictive value (NPV), and F1 scores surpassing 87% across all evaluation criteria. The KNN classifier displayed superior overall performance with the highest macro-averaged accuracy of 90.7%. These findings underscore the potential of Raman spectroscopy combined with ML as a robust and non-invasive technique for accurately discriminating BCC and its subtypes from normal skin tissues.

CİLT KANSERİNE BAĞLI CİLTTEKİ YEREL YAPISAL BOZULMALARIN RAMAN SPEKTROSKOPİSİ VE MAKİNE ÖĞRENMESİ İLE TESPİTİ

ÖZET

Küresel nüfusun önemli bir kısmı cilt kanseri ile mücadele etmektedir. Bu hastalık yaygınlığı ile bilinmekte olan ve potansiyel anlamda ölümcül bir hastalık olarak nitelendirilen bir hastalıktır. Epidemiyolojik verilerin analizi, cilt kanseri vakalarında dünya çapında endişe verici bir artış olduğunu ortaya koymakta ve sürekli olarak alınması gereken önlemlerin kritik önemini vurgulamaktadır. Erken teşhis, cilt kanserini etkili bir şekilde yönetmede ve hastalığın sonuçlarını istatistiksel olarak iyileştirmede kilit rol oynamaktadır. Özellikle cilt kanseri alanında hastalığın zamanında ve doğru bir şekilde tespiti hastalığın önüne geçilmesine imkan vererek birçok yaşamı kurtarma potansiyeline sahip olması nedeniyle sayısız biyomedikal uygulamada ve çeşitli tıbbi senaryolarda büyük önem taşımaktadır.

Farklı cilt kanseri türleri arasında, bazal hücreli karsinom (BHK) güneşe maruz kalan cilt bölgelerinde sıklıkla ortaya çıkan en yaygın tür olarak öne çıkmaktadır. BHK, yerel invazyon eğilimi ve yavaş büyüme özelliğiyle karakterize edilir ve potansiyel olarak metastaz yapabilir. Amerika Birleşik Devletleri'nde BHK ortalaması 100.000 kişi başına 300 vaka olup, yıllık artışın %10'u aşan bir orandadır. Görece düşük ölüm oranına rağmen, bu hastalık önemli bir nüfusu etkilemekte ve örneğin Birleşik Krallık sağlık sistemine önemli bir yük getirmektedir. BHK'nın tedavisi için geleneksel prosedürler genellikle etkilidir, ancak klinik değerlendirmelerin subjektif doğası, biyopsilerin invazif doğası ve teşhislerde gecikmeler gibi çeşitli dezavantajları bulunmaktadır. Buna karşın modern biyomedikal araştırmalar, ileri teknolojiler ve analitik metodolojilerden faydalanarak biyolojik analizlerde derinlemesine anlayış sağlayan yeni fırsatlar sunmaktadır.

Raman spektroskopisi son zamanlarda cilt hastalıklarını doğru bir şekilde tanımlama potansiyeline sahip alternatif bir yöntem olarak dikkat çekmektedir. Kısaca Raman spektroskopisi, bir malzemenin ışıkla olan etkileşimini gözlemleyen bir analiz tekniğidir. Özellikle bu çalışmada olduğu gibi moleküler yapıları belirlemek, farklılıkları ayrıştırmak için kullanılır. Bu teknikte, incelenecek yapıya lazer ışığı gönderilir ve yapıdan saçılan ışığın dalga boylarındaki değişiklikler gözlemlenerek malzemenin kimyasal bileşimi ve malzemenin yapısal özellikleri hakkında bilgi elde edilir. Raman spektroskopisinin makine öğrenimi teknikleri ile işbirliği ile ciltteki yerel yapısal bozulmaların teşhisi yapılabilir. Bu çalışmada Raman spektroskopisi ve çeşitli denetimli makine öğrenimi algoritmalarını kullanarak kanserden etkilenen dokunun normal doku ile ayrıştırılması ile birlikte BHK'nın alt tipleri olan nodüler BHK ve infiltratif BHK kanser tiplerinin ayırt edilmesi amaçlanmaktadır. Başarılı doku ayırımının patolojik teşhis sürecini azaltarak daha hızlı tanı oranlarına ve daha az ölüme yol açabileceği düşünülmektedir.

İstanbul Türkiye'de bulunan Şişli Hamidiye Etfal Eğitim ve Araştırma Hastanesi Etik Kurulu tarafından onaylanan bu prospektif çalışmada, BHK tanısı konmuş hastalar, “punch" biyopsi yoluyla histopatolojik teşhisi takiben deneyimli bir plastik cerrah tarafından total eksizyon işlemine tabi tutulmuştur. Çeşitli boyutlarda taze doku örnekleri fizyolojik sodyum klorür çözeltisi ile doldurulmuş bir kap içine dikkatlice yerleştirilmiş ve Raman spektroskopisi incelemesi için İstanbul Teknik Üniversitesi'ne taşınmıştır. Alüminyum folyo ile kaplanmış mikroskop camlarının Raman sinyallerini bastırması için özel numune tutucuları oluşturulmuş, bu da tekniği daha bütçe dostu hale getirmiştir. Taze dokular üzerinde Raman ölçümleri gerçekleştirilmiş ve daha sonra bu örnekler nodüler ve infiltratif BHK alt gruplarını tanımlayan deneyimli patologlar tarafından daha fazla incelenmek üzere güvenli bir şekilde hastaneye geri taşınmıştır.

Bir sonraki aşamada, henüz daha bir işleme tabi tutulmamış olan ham Raman verileri kapsamlı bir ön işlemden geçirilmiştir. İlk olarak, ham Raman verileri üzerinden kozmik ışınlar ortadan kaldırılmış, sonrasında her spektrumdaki floresans kaynaklı arka plan kaldırılmıştır. Daha sonra, Savitsky-Golay düzleştirme yöntemi her spektrumu pürüzsüzleştirmek için uygulanmış, gereksiz veri noktalarının ve beklenmedik bozucuların ortadan kaldırılması sağlanmıştır. Bir sonraki aşamada, her bir spektrum özelinde verinin düzenliliği amacı ile bir normalizasyon işlemi gerçekleştirilmiştir. Bu ön işlem adımları veri setini standartlaştırmakla birlikte gürültüyü ve değişkenliği azaltıp makine öğrenimi analizlerine hazır hale getirip, her spektrumun adil bir şekilde değerlendirileceği bir verisetinin oluşumunu sağlamıştır.

400 ile 3200 cm^{-1} arasındaki her Raman spektrumu için sınıflandırma tabanlı makine öğrenimi modelleri oluşturmadan önce, veri kümesi eğitim ve test alt kümelerine ayrılmış ve eğitim test kümesi %80 oranda ayrılmıştır. Aşırı öğrenmeyi azaltmak için, 5 katlı çapraz doğrulama kullanılmış ve her örnek için doğrulama skorları izlenmiştir. Makine öğrenmesinin sınıflandırma yapabilmek için kullandığı metrikler dokulardan elde edilen dalgaboyu-yoğunluk grafiklerinden de anlaşılabileceği gibi dokuların yoğunluk farklılıkları ve grafik üzerindeki pik noktalarında meydana gelen kaymalardır. Sınıflandırma süreci boyunca 7 farklı makine öğrenimi modeli kullanılmış olup, bu sınıflandırma modellernin farklı metriklerinin kullanılması da dahil toplamda 9 farklı modelin istatistiksel sonuçları incelenmiştir. Bu sınıflandırma modelleri arasında “Random Forest” (RF), “Decision Tree” (DT), “k-Nearest Neighbor” (KNN), “Logistic Regression” (LR), “Linear Discriminant Analysis” (LDA), “Multilayer Perceptron” (MLP) ve “Support Vector Machine” (SVM) bulunmaktadır.

Bu çalışmada sınıflandırma ve istatistiksel sonuçların incelenmesi iki farklı safhada yapılmıştır: İlk olarak, BHK ve normal dokuların ayrımı incelenmiş, ikinci olarak da nodüler BHK ve infiltratif BHK dokuları arasındaki ayrımın çıktıları gözlemlenmiştir.

BHK ve normal doku ayrımı için elde edilen sonuçlar, tüm makine öğrenimi tabanlı sınıflandırma modellerinde memnun edici istatistiksel metrik yüzdeleri sergilemiştir. Modeller arasında, RF ve KNN sınıflandırma modelleri diğer sınıflandırma modellerinin yüzdelerini geçmiş ve %98.4'lük doğruluk oranıyla en yüksek çıktı veren sınıflandırma modelleri olarak öne çıkmışlardır. Buna karşılık, LR ve LDA diğer sınıflandırma modellerinden daha düşük performans göstermiş olup doğruluk oranları sırasıyla %84.9 ve %84.6’dır. Ayrıca, RF sınıflandırma modeli, %98.4'lük makro-ortalama doğruluk yüzdesi ve %99'luk maksimum alan altı eğri skoru yüzdesi ile benzer performans sergilemektedir. Hem RF hem de KNN sınıflandırma modellerinde yüksek tutarlılık, yüksek doğruluk ve güçlü performans gözlenmiştir. BHK alt tiplerinin karşılaştırılması safhasında ise, elde edilen sonuçlarda hassasiyetin kısmen azalması gözlemlenmişken, çalışmanın makine öğrenimi sınıflandırma modellerinde nodüler BHK ve infiltratif BHK arasında doğruluk seviyesininin dikkate değer bir şekilde koruduğu görülmüştür. RF ve KNN sınıflandırma modelleri, sırasıyla %89.3 ve %90.7 doğruluk oranlarına ulaşarak alternatif modellerin önüne geçmiş ve olağanüstü bir performans sergilemiştir. Ayrıca, hem RF hem de KNN sınıflandırma modelleri, tüm değerlendirme kriterlerinde %87'nin üzerinde hassasiyet, özgüllük, pozitif öngörülen değer, negatif öngörülen değer ve F1 skoru değeri sergilemiştir. KNN sınıflandırma modeli, %90.7'lik makro-ortalama doğruluğa sahip olmuş ve üstün bir genel performans sergilemiştir. Bu bulgular, Raman spektroskopisinin makine öğrenimi ile birleştirilmesinin, yalnızca BHK ve normal cilt dokularının ayrımında başarılı bir yöntem olduğunu değil aynı zamanda BHK'nın alt tiplerinin ayrıştırılmasında da oldukça sağlam, güvenilir ve sürdürülebilir bir teknik olarak potansiyelini vurgulamıştır. Bu entegre yöntemin istatistiksel anlamda vermiş olduğu güven, BHK tabanlı cilt kanseri tanısının geleneksel yöntemlerden çok daha hızlı bir şekilde sağlanabileceğini göstermiş olup, bu sayede bu alandaki klinik yükün azaltılabileceğine ve BHK tabanlı cilt kanseri hastalığının ölüm oranının düşmesi konusunda oldukça ümit verici olmuştur.

1. INTRODUCTION

Nowadays, a considerable number of individuals globally affected with skin cancer, representing a pervasive and potentially fatal disease [1,2]. From the analyzed epidemiological data, observing a concerning rise in skin cancer cases globally, highlighting the importance of continued surveillance and preventive measures [3]. The escalating incidence of skin cancer correlates with heightened exposure to sunlight, ultraviolet light, environmental contaminants, and specific chemicals like arsenic and nitrates [4]. It has been demonstrated that there is a significant association between ambient UV radiation levels and the incidence of skin cancer [5]. The effective handling of skin cancer and the enhancement of patient prognoses relies on early diagnosis and accurate detection [6]. In numerous biomedical applications, including various medical contexts, timely detection holds crucial significance in addressing skin cancer, potentially saving numerous lives through effective treatment interventions. From the various forms of skin cancer, basal cell carcinoma (BCC) stands out as the most prevalent, often appearing on sun-exposed skin [7].

BCC is a locally invasive cancer that frequently grows slowly, yet it may spread [8, 9]. In the US, there are 300 cases of BCC for every 100,000 persons. There is a 30% lifetime risk as a result of the annual rate of rise exceeding 10%. The condition affects a large number of people despite having a low death rate, which puts a strain on the United Kingdom healthcare system [9]. BCC is usually diagnosed by a number of techniques, such as punch biopsy or excisional biopsy, dermoscopy, and visual inspection [10]. Although the usual procedures for BCC are often successful, there are many drawbacks to this approach, including the subjectivity of the clinical assessment, the invasiveness of the biopsy, and the delay in diagnosis. Through in-depth biological analysis, modern biomedical research creates new chances for understanding diseases by utilizing rapidly evolving technologies and analytical methodologies. As a potential substitute method for precisely identifying skin malignancies, Raman spectroscopy has recently gained popularity [11, 12]. Raman spectroscopy is a nondestructive method that provides comprehensive information about a substance's chemical structure. It has a wide range of applications in the fields of materials science, chemistry, biology, and medicine [13]. This multidisciplinary approach makes use of vibrational spectroscopy to reveal intricate chemical information and machine learning (ML) techniques to draw conclusions and patterns from large, intricate datasets. Consequently, it is possible to differentiate between malignant and healthy tissue using complementary methods involving Raman spectroscopy and ML. The integration of ML algorithms augments the diagnostic capabilities of Raman spectroscopy by facilitating the extraction of complex patterns and features from spectral data [14]. ML algorithms, such as Support Vector Machine (SVM), Random Forest (RF), and Artificial Neural Networks (ANN), can effectively classify Raman spectra based on distinctive spectral signatures associated with BCC pathology. Through the iterative process of model training and validation, ML algorithms can learn to discern subtle variations in spectral patterns indicative of pathological changes, thereby enabling accurate and automated diagnosis of BCC.

1.1 Purpose of Thesis

This study focuses on identifying local structural irregularities present in tissue affected by tumors relative to normal tissue, utilizing Raman spectroscopy in conjunction with diverse supervised ML algorithms. Additionally, the research delves into the differentiation of BCC subtypes, particularly distinguishing between nodular BCC and infiltrative BCC. To classify normal and BCC tissues, extensive Raman measurements are conducted across multiple locations within fresh tissue samples [15]. The successful discrimination of tissue types achieved in this study holds significant implications for reducing the pathological diagnosis phase, thereby expediting early recognition rates and subsequently mitigating mortality rates [16].

1.2 Significance of Thesis

The significance of this thesis lies in its discovery of an innovative approach to BCC skin cancer detection through the integration of Raman spectroscopy and ML techniques. Although BCC is one of the most prevalent types of skin cancer, it may present with subtle symptoms such as a small, shiny bump or a translucent pearly nodule that can easily be mistaken for a tissue condition or overlooked [17].

A rapid and noninvasive way to assess the biochemical content of a sample is to employ Raman spectroscopy, which may make it possible to identify BCC lesions early on [18]. In this study, the integration of ML algorithms trained on Raman spectroscopic data is employed to create a reliable and accurate diagnostic tool for the early identification of BCC. This integration can completely alter the diagnosis of BCC and ultimately result in better patient outcomes and lower medical expenses by providing physicians with a reliable and efficient way to differentiate between benign and malignant lesions.

2. LITERATURE REVIEW

A significant amount of research has been conducted lately on the application of ML and Raman spectroscopy to identify various types of cancer. This also produced a great deal of interest in creating advanced and accurate skin cancer diagnosis techniques.

2.1 Traditional Detection Strategies

In this study, to observe and investigate the early diagnosis of BCC the integration of Raman spectroscopy and ML algorithms is used. In the literature, there are various detection methodologies to diagnose.

Dermoscopy, alternatively referred to as dermatoscopy or epiluminescence microscopy, entails the utilization of a handheld device equipped with a magnifying lens and light source to scrutinize skin lesions. This technique enables a detailed examination of the skin surface, aiding dermatologists in discerning distinctive attributes associated with BCC, including arborizing blood vessels, ulceration, and pigmentary patterns [19]. Skin biopsy represents the gold standard in the diagnostic process of BCC. This procedure involves the extraction of a sample from the suspicious skin lesion, subsequently subjected to microscopic examination by a pathologist to ascertain the existence of malignant cells [20]. Reflectance confocal microscopy (RCM) stands as a non-invasive imaging modality offering high-resolution visualization of skin structures at a cellular level. This technique aids in discriminating between benign and malignant skin lesions, such as BCC, by facilitating the visualization of cellular structures and architectural features [21]. High-frequency ultrasound, recognized as ultrasound biomicroscopy (UBM) or high-resolution ultrasound (HRUS), serves as a valuable tool for evaluating the depth and scope of BCC lesions. This technique aids in assessing tumor thickness and invasion depth, crucial parameters influencing treatment strategies and prognostic considerations [22]. Regular photography and mole mapping entail the systematic documentation of the skin surface through the acquisition of comprehensive images.

These images serve as a baseline for tracking any alterations in skin lesions over successive examinations. By employing advanced digital imaging technologies, this approach aids in the timely identification of potentially concerning lesions and enables vigilant surveillance for indications of lesion development or reappearance [23].

2.2 ML-Based Detection Strategies

Nine biopsy specimens of perilesional skin and nine biopsy specimens of BCC were used to acquire Raman spectra in the investigation by Nijssen et al. According to the study, using spectral differences analysis and ML techniques like Principal Component Analysis (PCA) and Linear Discriminant Analysis (LDA), Raman spectroscopy was found to be a useful tool for differentiating between BCC and perilesional skin [24]. The study conducted by Choi and colleagues validates the efficacy of confocal Raman spectroscopy in the identification of dermatological conditions, specifically basal cell carcinoma. By successfully demonstrating the decrease in autofluorescence signals and highlighting the unique Raman band differences between normal and BCC tissues, their study highlights the feasibility of this technique as a noninvasive diagnostic tool that does not require a thorough statistical analysis of the spectral data. Additionally, their use of confocal Raman depth profiling demonstrated how well BCC tissue could be distinguished from nearby noncancerous tissue, offering a novel approach to direct spectral observations-based dermatological diagnosis [25]. In the Silveira et al. study, a linear least-squares fitting model was created to determine the relative spectrum effects of baseline biochemical components on the observed Raman signal, which was collected in vitro from both cancer and normal skin tissues. Ordinary least-square analysis was used to build the model, and an equation was used to determine each biochemical's estimated relative spectrum contribution [26]. Das et al. showed how ML may increase accuracy in skin cancer diagnosis by using deep convolutional neural networks and whole-slide imaging techniques. Furthermore, they investigated the application of artificial intelligence (AI) algorithms for self-skin assessment and carried out comparative analyses to evaluate the efficacy of ML in the diagnosis of skin cancer [27]. Mo et al. distinguished between malignant and healthy prostate tissues in humans by combining ML techniques with Stokes shift spectra. The Stokes shift spectra of fifteen pairs of pathologically confirmed human prostate cancer and normal tissues are combined in their investigation. PCA and nonnegative matrix factorization (NMF) were used for dimension reduction and feature detection after the spectra were produced. SVMs were then used to process the data. The findings showed that prostate tissue can be distinguished between benign and cancerous with a high degree of accuracy [28]. In order to diagnose colon cancer, Widjaja et al. used near-infrared (NIR) Raman spectroscopy with SVM-based multi-class classification models. The authors used datasets containing 105 tissue specimens for their investigation; these included 41 normal tissue specimens, 46 adenocarcinomas, and 18 hyperplastic polyps. By combining Gaussian radial basis function (RBF) C-SVM with NIR Raman spectroscopy, they were able to achieve an impressive diagnosis accuracy of 99.9% [29]. An overview of the use of ANN, SVM, Bayesian classification, partial least-squares regression, and multiple ensemble techniques in the diagnosis of diseases in the human body is given by Krafft et al. Epithelial tumors, brain tumors, prion diseases, bone illnesses, skin tumors, renal diseases, gallstones, diabetes, and osteoarthritis were among numerous disease topics included in the study. According to the findings of their investigation, techniques based on IR and Raman spectroscopy will soon become essential clinical instruments [30]. The implementation of deep learning techniques in dermatological diagnostics, namely in the diagnosis of skin cancer, has been studied by Campanella et al. Research integrating reflectance confocal microscopy (RCM) and convolutional neural networks (CNNs), a kind of deep learning model for image processing, has shown promise in distinguishing between skin lesions. Building on this basis, the proposed deep learning-based AI model for automatic BCC detection contributes to the growing body of research that shows how deep learning techniques can be used to improve the specificity and accuracy of skin cancer diagnoses by utilizing cutting-edge imaging technologies like RCM [31]. Spectral shift assessment-based optical imaging is utilized in a study by Niazi et al. to differentiate between normal and malignant skin tissues. Scientists identified distinct spectrum alterations that correlated with different skin diseases by analyzing fluorescence spectra pixel by pixel and identifying fluorescence peaks. In addition, the acquired data was processed using denoising techniques, which included the application of Gaussian filters, to enhance image clarity and minimize spurious signals. These methods, used in conjunction with data smoothing and signal processing approaches, helped correctly identify between healthy and afflicted tissues based on their spectral features [32]. In a different study by Serhantzov et al., researchers utilize autofluorescence and Raman Spectroscopy to enhance the quality of skin tumor differentiation while applying traditional ML approaches. Based on previous research on the use of ML in medical diagnostics, namely in the classification of skin cancer, the work is in line with a history of studies employing in vivo data collection techniques. The usage of Classification and Regression Tree (CART), Support Vector Classification (SVC), Logistic Regression (LR) and K-Nearest Neighbors (KNN) for the goal of diagnosing skin cancer using Raman spectra is in line with current methods examined in the literature [33].

3. METHODOLOGY

3.1 Sample Preparation

This prospective study was approved by the ethics committee of Şisli Hamidiye Etfal Training and Research Hospital in Istanbul, Türkiye. First, patients were examined by expert dermatologists and histopathologically diagnosed with BCC using a punch biopsy. Patients were referred to an experienced plastic surgeon after receiving a histological diagnosis, and the specialist carefully carried out total excision to remove the tissues. Then, the expert physician carefully placed the extracted tissue samples, which came in different sizes, in a closed container with gauze saturated in physiological sodium chloride solution (0.9%). The container was then transferred straight to Istanbul Technical University (ITU). At the ITU Nanotechnology Application and Research Center, tests using Raman spectroscopy were performed on fresh tissue samples that were both malignant and normal. Sample holders made to order were first produced in order to perform Raman measurements on fresh tissue samples. A microscope slide was coated with aluminum foil intended for kitchen use in order to suppress the Raman signal that the slide produced because metals are Raman passive. Utilizing this straightforward yet inventive technique is more affordable than using expensive microscope slides. Following the preparation of the specially made sample container, new tissues were carefully positioned above it and loaded underneath the Raman objective to obtain spectrum data. After Raman measurements, the tissues were placed in a secure container filled with formalin liquid and safely sent to the hospital so that skilled pathologists could examine them further that same day. The pathologists assessed the tissues and identified the nodular and infiltrative BCC subgroups.

In Figure 3.1, images of (a) nodular and (b) infiltrative BCC subtypes, each surrounded by normal skin tissue, are shown with tissue specimens removed by a plastic surgeon. Dermatologists have identified Raman probe areas, which are indicated by dashed circle lines in red and yellow. On fresh tissue samples, a variety of Raman spectra were obtained from those particular regions.

Figure 3.1 (c), (d), and (e) display the corresponding hematoxylin and eosin (H&E) images of nodular BCC, infiltrative BCC, and normal skin tissue, respectively. Following Raman measurements, two pathologists conducted a histopathologic evaluation.

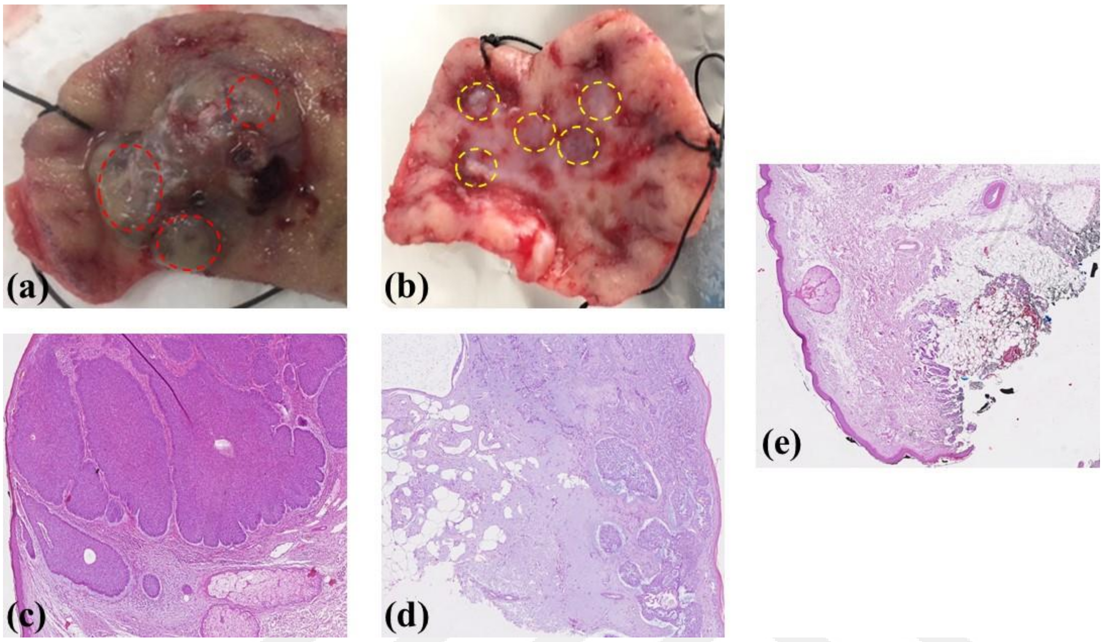

Figure 3.1 : Representation of tissue specimens and measurement protocol.

3.2 Raman Spectroscopy

An effective analytical method for examining the molecular vibrational modes in a substance is Raman spectroscopy. It is based on the inelastic scattering of monochromatic light by molecules within a sample, usually from a laser source. The majority of light that interacts with a molecule is elastically scattered, or Rayleigh scattered, meaning that it keeps the same wavelength and energy as the incident light. Yet, a low percentage of the dispersed light experiences inelastic scattering, which causes a frequency change called the Raman shift. The energy of the molecular vibrations inside the sample is reflected in this shift [34].

Plotting the intensity of the Raman scattered light as a function of the Raman shift yields the Raman spectrum, which offers important details on the molecular structure, bonding environment, and chemical makeup of the substance being studied. The Raman spectrum enables the identification of distinct chemical species and the characterization of molecular conformations by use of a peak that corresponds to a particular vibrational mode of the molecules present in the sample [35].

Compared to other spectroscopic methods, Raman spectroscopy has a number of advantages. It can be carried out in situ, in ambient or harsh environments, and under a variety of experimental conditions. It is also non-destructive and requires little sample preparation. Raman spectroscopy is a useful instrument for researching polymorphs, crystal defects, and chemical reactions in the fields of materials science, biology, environmental science, and pharmaceuticals. It is also sensitive to minute changes in molecular structure [36]. With the introduction of cutting-edge instruments like resonance Raman spectroscopy, surface-enhanced Raman spectroscopy, and confocal Raman microscopy, the technique has advanced significantly in recent years, increasing its applicability and improving its sensitivity and spatial resolution [37]. In both academic and industrial settings, Raman spectroscopy is still a very effective and adaptable analytical tool for characterizing and analyzing a wide range of materials and substances [38].

3.3 Raman Spectroscopy Instrumentation

Before taking measurements, the Raman spectroscopy system (Renishaw in Via Raman spectrometer, UK) was first calibrated using a silicon sample. A confocal Raman spectroscopy with an output power of 300 megawatt and a central wavelength of 785 nanometer was used to perform the Raman measurements. Throughout every measurement, the laser power is at 100%. Using an L50X objective with a numerical aperture of 0.5, the laser light was directed onto the fresh tissue samples, producing a spot size of about 2 micrometers. 10 seconds of exposure time and one accumulation were used to obtain Raman spectra. Using a step unit of 0.1 cm^{-1}, the chosen Raman spectrum range was 400 cm^{-1} to 3200 cm^{-1}. Throughout the course of the study, 52 spectra were obtained. Every Raman spectrum was gathered at room temperature.

3.4 Data Preprocessing

The Raman data output in this study was underwent extensive preprocessing steps to ensure its suitability for further analysis. In the study, Python (version 3.8), Origin Pro (Educational version 2022b–9.95), and MATLAB (Educational version R2023b) were the main tools used for the data preprocessing. Figure 3.2 displays the flowchart of the entire suggested methodology to differentiate between BCC and normal skin in addition to BCC subtypes. The instrument's cosmic rays were first eliminated after obtaining the raw Raman data. After the removal of cosmic rays, each spectrum's background caused by fluorescence was eliminated. Each detrended spectrum was then refined using the Savitsky-Golay smoothing method [39], which included a second-order polynomial and a five-point filter. The elimination of unnecessary data points and the avoidance of unforeseen noises were guaranteed by this smoothing process. Normalization followed on each spectrum to provide uniformity and comparability across the various spectral profiles. The dataset was standardized and noise and volatility were reduced by these consecutive steps, preparing it for reliable ML analysis.

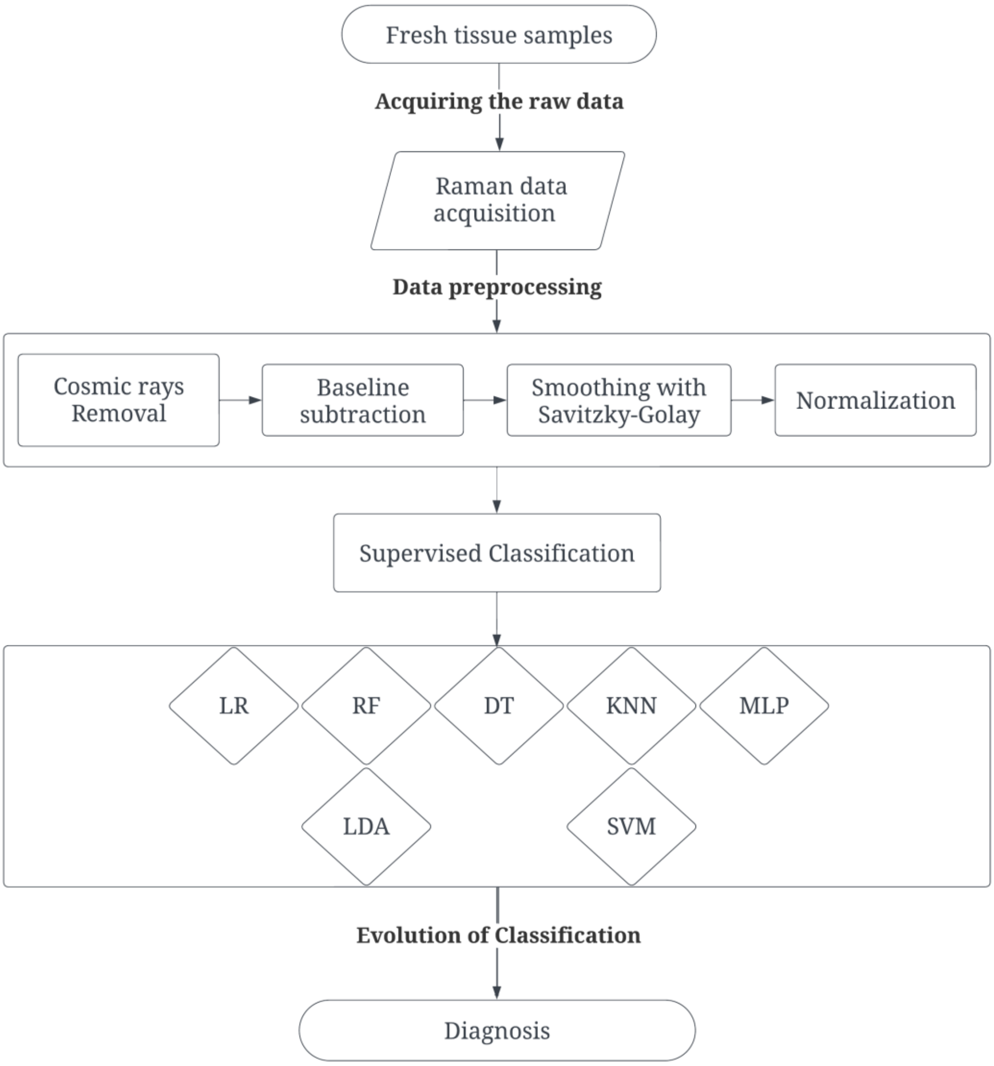

Figure 3.2 : Diagram illustrating the proposed process for diagnosis by Raman spectroscopy and ML.

3.5 Classification Models and Evaluation Metrics

In ML, classification is the process of categorizing input data into predetermined groups. Its main goal is to correctly identify an instance by analyzing incoming data using a trained model. Pre-labeled training data is used in the classification process, with each instance within a sample set being linked to the correct class label. Using this labeled dataset, a model learns to correlate input attributes with matching class labels.

A vital component of ML is supervised classification models, which are distinguished by their dependence on labeled training data to forecast the class labels of cases that have not yet been encountered. Each training sample in supervised classification consists of a set of characteristics and a corresponding class label, giving the model explicit knowledge of the appropriate output for every input occurrence [40]. Through training, these models hope to understand the relationship between input features and class labels, which will allow them to predict new, unlabeled data with accuracy. Supervised classification uses a variety of algorithms, each with unique advantages and disadvantages [41].

Metrics including accuracy, precision, recall, F1-score, and receiver operating characteristic (ROC) curve analysis are frequently used to assess the effectiveness of supervised classification models. Furthermore, methods such as cross-validation are utilized to evaluate the generalization of the model on new data and reduce overfitting. Although supervised classification models are effective, they need a large enough amount of labeled data to be trained, and the diversity and representativeness of the training dataset have a significant impact on the accuracy of the predictions. Therefore, developing reliable supervised classification systems requires rigorous feature engineering, data preparation, and model selection.

Before creating classification-based ML models for every Raman spectrum between 400 and 3200 cm^{-1}, the dataset was split into training and testing subsets, accounting for 80% of the total. In order to reduce overfitting, 5-fold cross-validation was also used and validation scores are observed for each instance [42]. In the study, the following ML models are utilized: RF, Decision Tree (DT), KNN, LR, LDA, Multilayer Perceptron (MLP), SVM.

3.5.1 Random forest classification model

In the Random Forest ensemble learning technique, multiple decision trees are used for classification and regression tasks. Using a bootstrapped sample of the training data and a random collection of features, each tree in the forest is constructed. When making a prediction, every tree produces its output individually. For classification tasks, the final forecast is determined by taking the mode of these outputs; for regression tasks, the average prediction is used. Random Forests are renowned for their adaptability to a wide range of uses, resilience to overfitting, and capacity for handling high-dimensional data [43]. Each decision tree in the Figure 3.3 is trained on a subset of the dataset, and the final result is generated by averaging or majority voting the individual results, thus taking advantage of the wisdom of the crowd for improved performance.

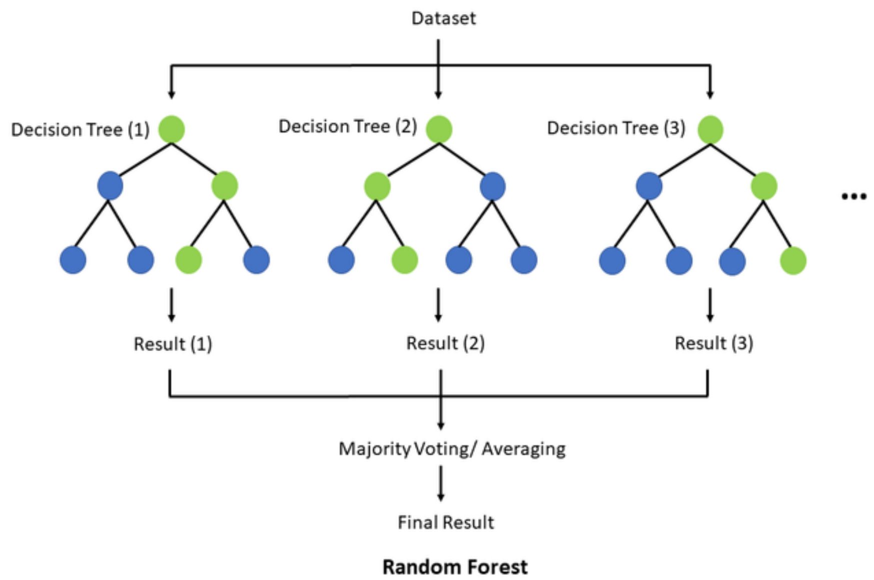

Figure 3.3 : RF Classification Model Architecture.

3.5.2 Decision tree classification model

A decision tree classification model is a type of predictive modeling in which the feature space is divided into a hierarchy of decision nodes, each of which reflects a selection made in response to a feature value. Recursively, the tree begins at the root node and divides the data into smaller subsets according to the characteristic that best distinguishes the classes, as evaluated by factors like information gain or Gini impurity [44]. This procedure is repeated until each final node's data is primarily of a single class, at which point the leaf nodes are formed. An instance is given the class label linked to the majority of instances in the leaf node as it moves through the tree from the root to a leaf while prediction is in progress. Decision trees are widely utilized in many different sectors because they are interpretable, simple to comprehend, and capable of capturing complicated relationships in the data [45].

To demonstrate decision tree algorithm's working methodology mathematically, explaining the Gini impurity can be a feasible start. Gini impurity calculates the degree of impurity in a node. For a node t containing N_t samples, where p_{ti} is the proportion of instances of class i in node t, the $G(t)$ – Gini impurity is calculated as follows:

$$G(t) = 1 - \sum_{i=1}^{c}(p_{ti})^2 \tag{3.1}$$

Where c is the number of classes.

To evaluate the effectiveness of a split in a decision tree, information gain is used. Given a parent node t with Gini impurity $G(t)$ and child nodes t_{left} and t_{right} resulting from a split, the information gain IG is calculated as:

$$IG(t) = G(t) - \left(\frac{N_{left}}{N_t}\right)G\left(t_{left}\right) + \frac{N_{right}}{N_t}G(t_{right}) \tag{3.2}$$

Where N_{left} and N_{right} are respectively the number of instances in the left and right child nodes.

Recursively, the decision tree divides the data according to the characteristic that reduces impurity or maximizes information gain. Assume that *split value* is a threshold value for feature X_i, and that X_j is the *j-th* feature. The condition for splitting is:

$$split\ value\ = argmax_{X_j} IG(t) \tag{3.3}$$

When specific stopping conditions are satisfied, such as a maximum depth, a minimum number of samples per leaf node, or the process of gathering no more information, the tree-growing process ends.

Based on the choices taken at each split, a new instance moves through the tree during prediction, moving from the root to a leaf node. The majority class among the samples in the leaf node is the anticipated class label for the instance [46].

3.5.3 K-nearest neighbors classification model

It is a classification model that is an efficient yet straightforward technique for both classification and regression problems. When a fresh and unlabeled instance is introduced to the KNN classification method, it finds the *K* nearest labeled instances (neighbors) in the training set using a distance metric (such as the Euclidean distance) in the feature space. The new instance is then given the class label of most of these *K* neighbors, which is a well-known example of instance-based or lazy learning [47]. KNN uses the complete training dataset for classification rather than explicit training. It can handle non-linear decision boundaries and is simple to learn and intuitive. However, the distance metric and K selection may have an impact on how well it performs [48]. Furthermore, the presence of irrelevant or noisy features in the dataset and the feature scaling selection can have an impact on KNN's performance, underscoring the significance of data preprocessing steps in maximizing its efficacy.

3.5.4 Logistic regression classification model

Logistic regression classification model is a popular linear classification technique for simulating the likelihood of a binary result. Using a logistic function, frequently referred to as the sigmoid function, logistic regression calculates the likelihood that a given instance fits into one of the two classes given a collection of input data. The logistic function is used to determine the probability of the positive class once the model learns the weights associated with each feature. The weights then combined linearly with the feature values. During training, the logistic loss function, which penalizes deviations between the predicted probabilities and the actual class labels, is minimized by optimizing the model's parameters using methods like maximum likelihood estimation or gradient descent.

As it is known in the previous studies, logistic regression classification methodology is widely used in medical area [49]. Since it is simple to comprehend, straightforward, and capable of handling both linearly and non-linearly separable datasets with appropriate feature engineering or transformation, logistic regression is a common statistical technique [50].

3.5.5 Linear discrimination analysis classification model

An approach for classification called linear discriminant analysis looks for linear feature combinations that optimally divide the data's classes. It is assumed that each classes data have a shared covariance matrix, class-specific means, and a normally distributed distribution. The posterior probability of each class given an input instance is then calculated using the Bayes theorem via LDA after calculating the class means and covariance matrix estimations. Classification is predicated on placing the instance in the class with the highest posterior probability, and the decision boundary between classes is linear. LDA is frequently used in practice since of its simplicity and interpretability; it is especially helpful when the classes are well-separated and the assumption of normality holds true [51].

3.5.6 Multilayer perceptron classification model

A type of artificial neural network called a multilayer perceptron classification model has several layers of connected neurons. An activation function is applied by each neuron in the network to the weighted sum of its inputs, resulting in an output that is forwarded to the subsequent layer. The network typically contains one or more hidden layers between the input and output layers. The model uses backpropagation to determine the ideal weights and biases during training. These are then modified to minimize a given loss function, such as categorical cross-entropy, between the predicted and actual class labels. MLPs are appropriate for a variety of classification positions due to their great flexibility and capacity to learn complex nonlinear correlations in the data. However, they are prone to overfitting with little data or too complicated topologies, and they can need careful hyperparameter adjustment [52]. In the Figure 3.4, MLP receives four input features, processes them via a neuronal hidden layer, and outputs a single feature. Due to the weighted connections between each neuron in the hidden layer and every input and output layer, the network is able to learn intricate patterns.

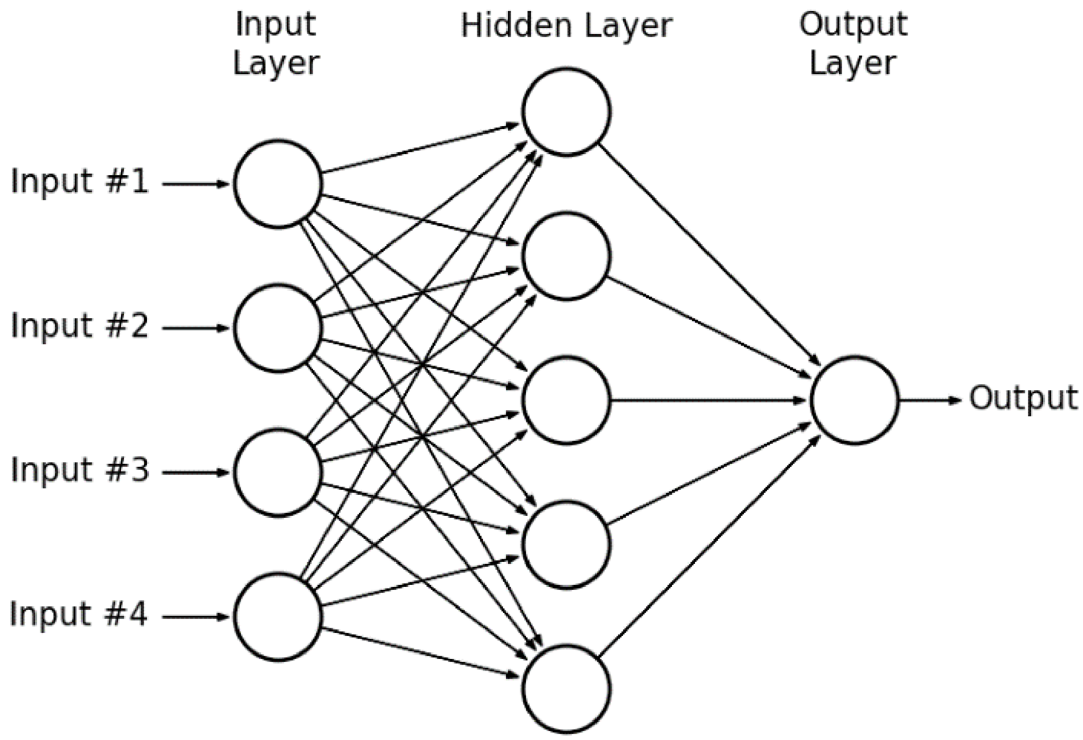

Figure 3.4 : Architecture of a MLP Network.

3.5.7 Support vector machine classification model

Support Vector Machine is a strong classification model that focuses to acquire the optimal hyperplane that splits the classes in the feature space while maximizing the margin between the classes. Using a kernel function, SVMs translate the input features into a higher-dimensional space where the data may be linearly separable. The model locates the hyperplane, or support vector, that optimizes the margin between the closest occurrences of various classes in this higher-dimensional space. These support vectors establish the decision boundary, and fresh instances are classified according to their location on the hyperplane. SVMs can handle high-dimensional data effectively and work well with datasets that are both linearly and non-linearly separable. They can be computationally expensive for large datasets, though, and are dependent on the regularization settings and kernel function selected [53]. The dashed lines in the Figure 3.5 indicate the margins, and the red line in the figure represents the hyperplane. The location and orientation of the hyperplane are determined by the closest data points (support vectors) on either side of the margin.

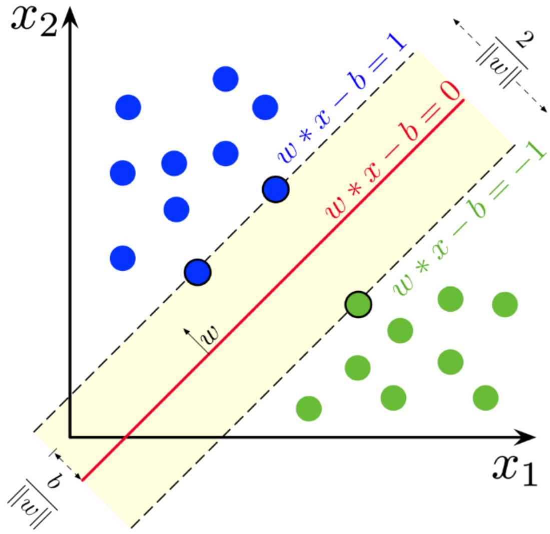

Figure 3.5 : Maximum-margin hyperplane and margins for a SVM trained on two classes of samples.

4. RESULTS AND DISCUSSION

A comprehensive review of tissue samples obtained from patients with BCC, a prevalent form of skin cancer with a variety of clinical manifestations, is provided in this section. Two major topics are covered in depth in this thesis: first, a thorough analysis of the normal tissue surrounding BCC lesions provides insight into the microenvironment and possible biomarkers linked to tumorigenesis; second, a thorough investigation of various BCC tissue subtypes clarifies the molecular signatures and histopathological differences that underlie this diverse cancer. By utilizing meticulous histological evaluation, immunohistochemical staining, and molecular profiling techniques, the objective is to unravel the complex interactions among genetic modifications, tumor microenvironment, and clinical consequences in BCC. This will enhance our comprehension of the disease's etiology and facilitate the development of focused therapeutic approaches.

4.1 Normal – Basal Cell Carcinoma Tissue Analysis

Figure 4.1 indicates the normalized mean Raman spectra of noninvasive tissues (black-solid lines) and BCC tissues (red-solid line). Besides, yellow-solid line demonstrates the corresponding absolute difference between these two normal and BCC intensities. From 400 to 3200 cm^{-1}, the ex vivo fresh tissue Raman observations span a broad spectral range that includes both low and high wavenumber regions. The high wavenumber region (2800−3020 cm^{-1}) records CH-stretching spectroscopic information, which is essential for examining protein and lipid vibrations [54], while the low wavenumber region correlates to the biological fingerprint region [55]. The skin's spectral features indicate distinctive peaks that resemble those reported in the literature [24, 56, 57, 58]. Figure 4.1's difference spectrum shows differences in the mean BCC spectrum and mean normal spectrum in the high wavenumber region as well as the biological fingerprint region.

The fingerprint region is where the most pronounced variations in Raman peak intensity are seen; in particular, BCC exhibits lower Raman peak intensities around 536 cm^{-1} and 853 cm^{-1}, while higher Raman peak intensities around 937 cm^{-1}, 1004 cm^{-1}, 1318 cm^{-1}, and 1449 cm^{-1} in comparison to the normal spectrum. However, over the whole high wavenumber range, BCC shows noticeably less Raman intensity than the normal spectrum.

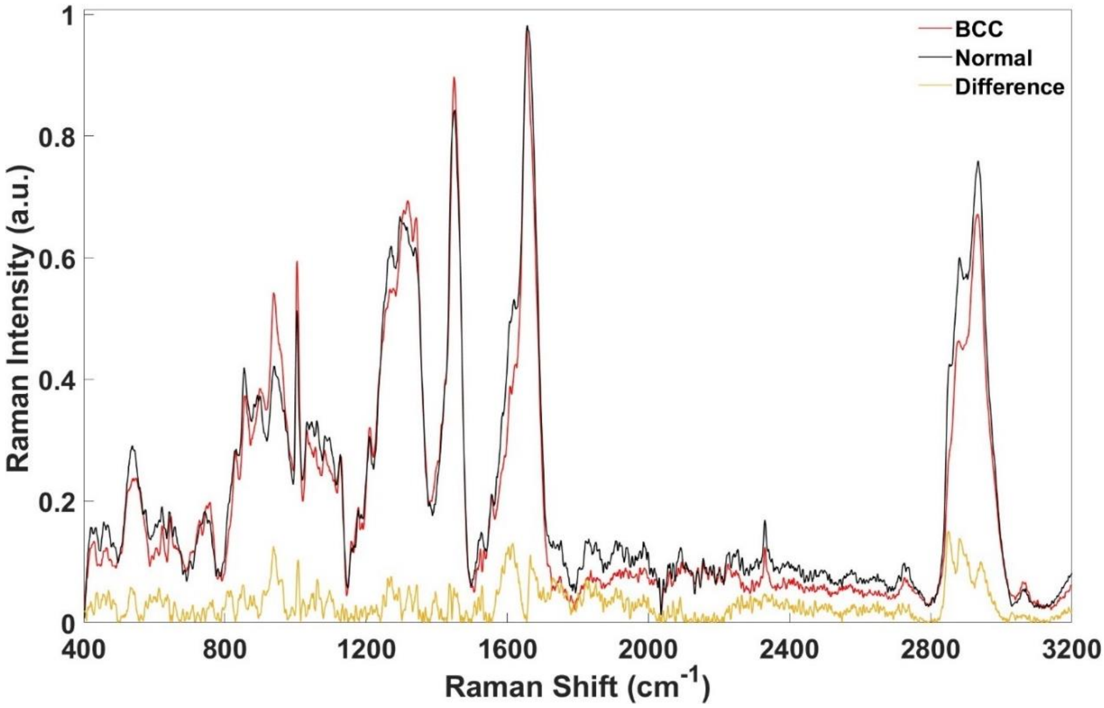

Figure 4.1 : Noninvasive skin (black-solid line) and normalized mean Raman spectra of BCC (red-solid line) tissues.

Furthermore, six peak positions (~536 cm^{-1}, 743 cm^{-1}, 853 cm^{-1}, 1295 cm^{-1}, 1618 cm^{-1}, and 2882 cm^{-1}) with significant Raman shifts between the normal skin spectrum and the BCC spectrum are found, as shown in Figure 4.2 (spectra modified for clarity). The Raman peak position of the BCC spectrum shifts from around 1295 cm^{-1} to 1318 cm^{-1} in relation to the normal skin spectrum at a location that is the most noticeable shift in peak position. The CH_2 distortion is attributed to this peak, which could potentially function as a distinguishing factor between BCC and noninvasive skin tissue.

In Figure 4.2 vertical dashed lines shows the relative Raman shift peak positions between the spectra. Dashed lines correspond which peaks are shifted clearly, and the value top of them indicates the Raman shift wavelengths for each dashed line.

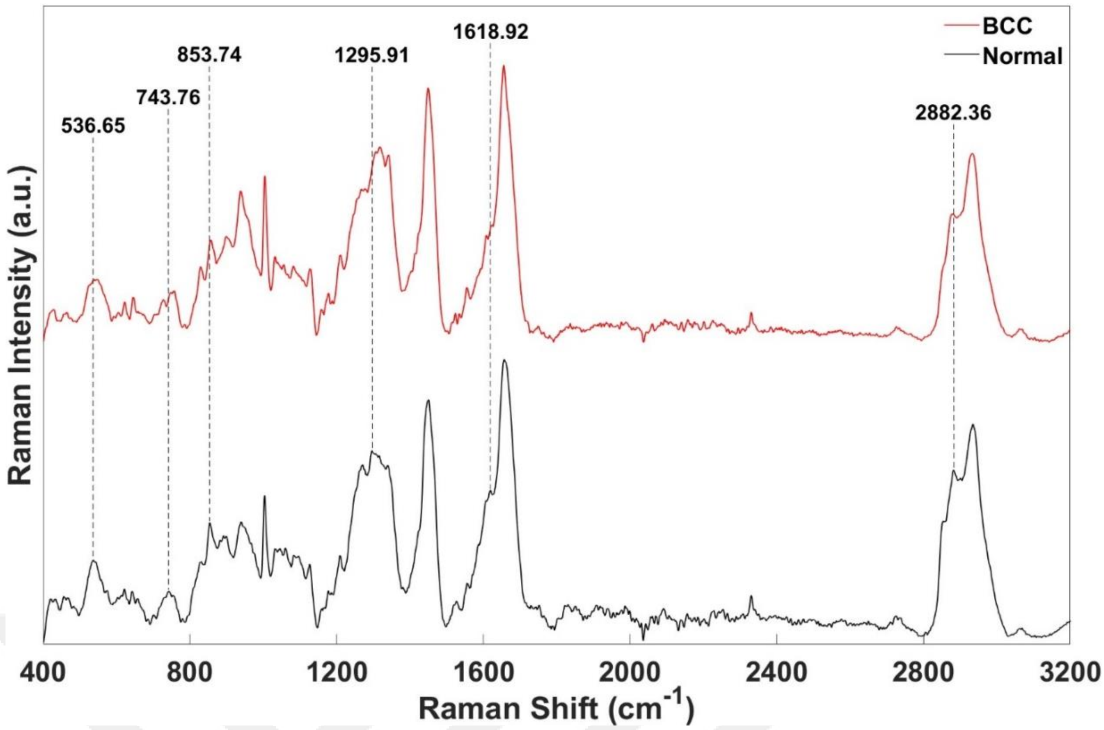

Figure 4.2 : Mean Raman spectra and peak shift points of normal (black-solid line) and BCC (red-solid line) skin tissues.

The information on these spectral peak positions in Figure 4.2 is indicated in Table 4.1. These variations in the Raman peak's intensity and position support the altered molecular structure of BCC compared to normal skin. These differences therefore indicate that Raman spectroscopy can be useful for the accurate detection of local molecular structural distortions in skin caused by BCC tumors.

Table 4.1 : Raman shift peak positions in BCC and normal skin tissues assignments.

Raman shift peak positions (cm^{-1})	Raman band assignments	References
36 cm^{-1}	S-S bond stretching (cysteine) in proteins (actin, collagen and elastin); glucose/glycogen	59
541 cm^{-1}	S-S bond stretching (cysteine) in proteins (actin, collagen and elastin); glucose/glycogen	59, 60
743 cm^{-1}	Symmetric breathing of tryptophan	60, 61
853 cm^{-1}	CCH bending (aromatic) of proteins	62, 63, 64, 65
897 cm^{-1}	Unassigned	
1277 cm^{-1}	Amide III (α-helix conformation)	60, 62, 63, 65, 66
1295 cm^{-1}	CH_2 deformation	62, 66
1339 cm^{-1}	CH vibrations (CH_2 and CH_3 wagging)	63, 66
1618 cm^{-1}	Red blood cells (heme group); C=C modes (stretching/bending) of tyrosine, tryptophan and phenylalanine in proteins (actin and elastin)	60
2880 cm^{-1}	CH_2 symmetric stretch of lipids	66, 67
2882 cm^{-1}	CH_2 asymmetric stretch	66, 68
2931 cm^{-1}	CH_3 stretching (protein)	61, 67

Following, after spectral analysis is demonstrated, the preprocessed Raman data is combined with numerous supervised ML classification models to successfully discriminate the diseased skin tissue from normal skin tissue, with their performance evaluated by various statistical evaluation metrics. In Table 4.2, confusion matrices for each supervised classification methodology are shown. The confusion matrix arguments are used to evaluate the performance of the ML models. The evaluation metrics are computed in terms of true positive, true negative, false positive, and false negative parameters for each classification model, as indicated in Table 4.3. Furthermore, Table 4.4's macro-averaged metrics provide an overall picture of each supervised classifier's performance. Figure 4.3 shows the ROC curves for all models. In the following tables PPV refers to “Positive Predictive Value”, NPV refers to “Negative Predictive Value”.

Table 4.2 : Confusion matrices for BCC and normal skin tissues by each supervised classifier.

Supervised Classification Models	Confusion Matrix		
	Classes	Normal	BCC
RF	Normal	579	13
	BCC	5	594
DT	Normal	591	21
	BCC	36	543
KNN (K=5)	Normal	598	11
	BCC	7	575
RF (with PCA, n = 3)	Normal	553	37
	BCC	62	539
LR	Normal	501	102
	BCC	77	511
LDA	Normal	508	98
	BCC	85	500
MLP (L = 8)	Normal	514	74
	BCC	67	536
SVM (C = 5)	Normal	522	88
	BCC	40	541
SVM (C = 100)	Normal	557	45
	BCC	27	562

Table 4.3 : Evaluation metrics by each supervised classifier for BCC and noninvasive skin tissues.

	Evaluation Metrics						
	Classes	Accuracy	Sensitivity	Specificity	PPV	NPV	F1 Score
RF	Normal	0.984	0.991	0.978	0.978	0.991	0.984
	BCC	0.984	0.978	0.991	0.991	0.978	0.985
DT	Normal	0.952	0.942	0.962	0.965	0.938	0.954
	BCC	0.952	0.962	0.942	0.937	0.965	0.95
KNN (K=5)	Normal	0.984	0.988	0.981	0.981	0.988	0.985
	BCC	0.984	0.981	0.988	0.988	0.981	0.984
RF (with PCA, n = 3)	Normal	0.916	0.899	0.935	0.937	0.896	0.917
	BCC	0.916	0.935	0.899	0.896	0.937	0.915
LR	Normal	0.849	0.866	0.833	0.83	0.869	0.848
	BCC	0.849	0.833	0.866	0.869	0.83	0.851
LDA	Normal	0.846	0.856	0.836	0.838	0.854	0.847
	BCC	0.846	0.836	0.856	0.854	0.838	0.845
MLP (L = 8)	Normal	0.881	0.884	0.878	0.874	0.888	0.879
	BCC	0.881	0.878	0.884	0.888	0.874	0.883
SVM (C = 5)	Normal	0.892	0.928	0.86	0.855	0.931	0.89
	BCC	0.892	0.86	0.928	0.931	0.855	0.894
SVM (C = 100)	Normal	0.939	0.953	0.925	0.925	0.954	0.939
	BCC	0.939	0.925	0.953	0.954	0.925	0.939

Table 4.4 : Macro-averaged metrics by each supervised classification method for BCC and noninvasive skin tissues.

	Macro-averaged Metrics					
	Accuracy	Sensitivity	Specificity	PPV	NPV	F1 Score
RF	0.984	0.985	0.985	0.985	0.985	0.985
DT	0.952	0.952	0.952	0.951	0.952	0.952
KNN (K=5)	0.985	0.985	0.985	0.985	0.985	0.985
RF (with PCA, n = 3)	0.917	0.918	0.918	0.917	0.917	0.917
LR	0.850	0.850	0.850	0.850	0.850	0.850
LDA	0.846	0.846	0.846	0.847	0.847	0.846
MLP (L = 8)	0.882	0.882	0.882	0.882	0.882	0.882
SVM (C = 5)	0.893	0.894	0.894	0.893	0.893	0.893
SVM (C = 100)	0.940	0.940	0.940	0.940	0.940	0.940

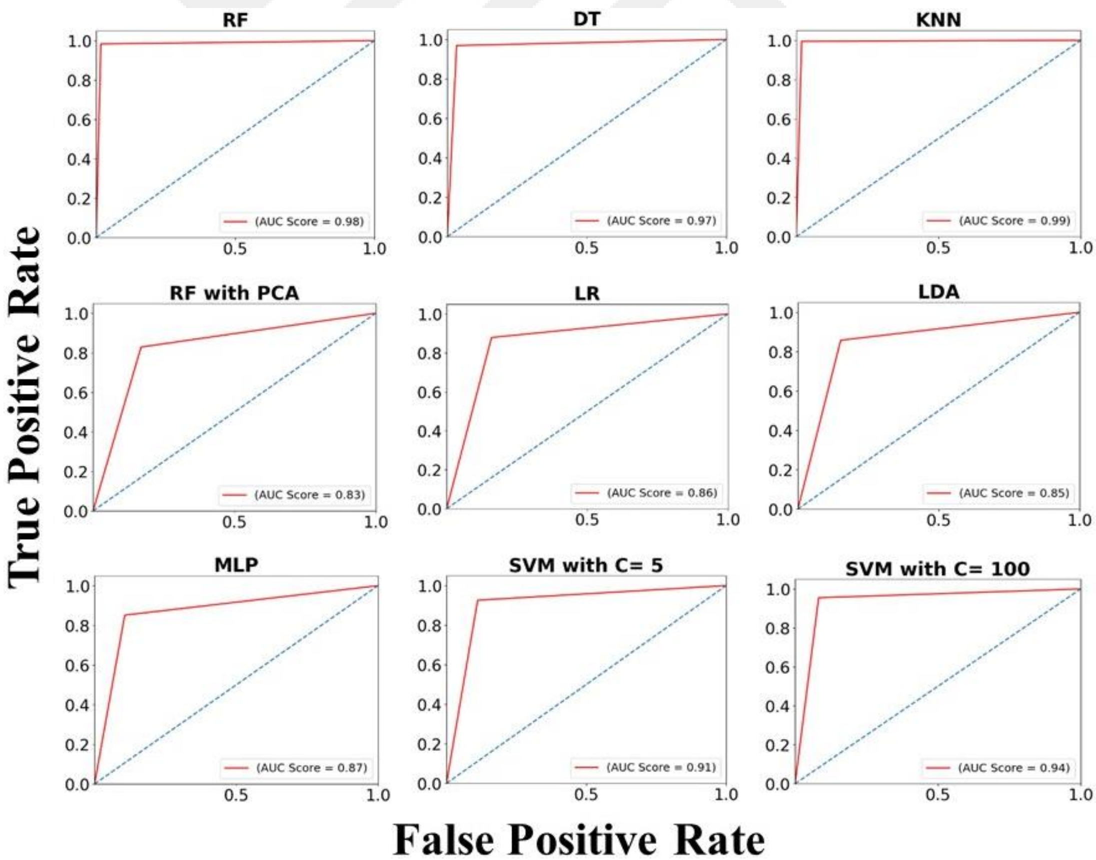

Figure 4.3 : ROC Curves of Classification Models for BCC and normal skin tissues.

The results indicate that all ML-based classifiers produce adequate metrics for separating BCC from normal skin, as shown in Table 4.3. With an accuracy of 98.4% compared to the other models, RF and KNN classifiers produced the best outcomes of all the models. Yet, it is observed that the LR and LDA provide the lowest performance with an accuracy of 84.9% and 84.6%, respectively. Referring to Table 4.4, results expose that the KNN classifier shows the best overall performance, with the finest macro-averaged accuracy of 98.5%. This model also ensures superior performance metrics: a sensitivity of 98.5%, a specificity of 98.5%, a PPV of 98.5%, an NPV of 98.5%, and an F1 score of 98.5%. Similarly, RF classifiers shows comparable performance metrics with the best macro-averaged accuracy of 98.4%. The RF classifier achieves the maximum area under curve (AUC) score of 99% in relation to the ROC curve which is shown in Figure 4.3. Also, it is apparent from Tables 4.2, 4.3, and 4.4 that both RF and KNN consistently display high accuracy and robust performance. By decreasing false positive and negative numbers in both classes, they also successfully strike a solid balance between sensitivity and specificity.

4.2 Subtypes of Basal Cell Carcinoma Tissues Analysis

Furthermore, the study is further advanced to not only examine the differences between BCC and normal cell types but also to dissect the variances among different types of BCCs, particularly nodular BCC and infiltrative BCC, using Raman spectroscopy along with supervised ML algorithms. Figure 4.4 indicates the normalized mean Raman spectra of nodular BCC (magenta-solid line) and infiltrative BCC (burgundy-solid line). It is noticed that the Raman peak intensity for nodular BCC is numerically greater for all peaks, with the exception of the peak at 856 cm^{-1} compared to infiltrative BCC in the fingerprint region. Nevertheless, infiltrative BCC displays elevated peak intensity compared to nodular BCC across the entire high wavenumber spectrum. To demonstrate the Raman peak shift, Figure 4.5 displays the average Raman spectra of nodular BCC and infiltrative BCC. To enhance clarity, the spectra are vertically shifted relative to each other. Additionally, six distinct peak positions (~541 cm^{-1}, 897 cm^{-1}, 1277 cm^{-1}, 1339 cm^{-1}, 2880 cm^{-1}, and 2931 cm^{-1}) showing notable variances between nodular and infiltrative spectra were identified. The most notable shifts in peak position are observed around ~ 541 cm^{-1} and 1277 cm^{-1}, with the Raman peak position of infiltrative BCC shifting to approximately ~ 531 cm^{-1} and 1268 cm^{-1}, respectively, compared to nodular BCC. The table also includes the spectral peak positions. Histopathologically, nodular type BCC is distinguished by the existence of sizable islands or clusters of malignant basaloid cells. These cells exhibit palisading along the edges and a disorderly arrangement within the cores of the islands. Conversely, unique histological characteristics are noted in infiltrating type BCC, characterized by elongated strands of basaloid cells, typically ranging from five to eight cells in thickness. These strands infiltrate between collagen bundles and may also exhibit a nodular component, as depicted in the case (Figure 3.1-d) [69]. Although both subtypes consist of basaloid cells, Raman spectroscopy can reliably distinguish between infiltrative and nodular BCC with high sensitivity and specificity. This capability is likely due to its capacity to assess the density and distribution of basaloid cells and to detect variations in cell texture. The noted disparities in both intensity and position of the Raman peaks support the local molecular structural differences between nodular and infiltrative BCC.

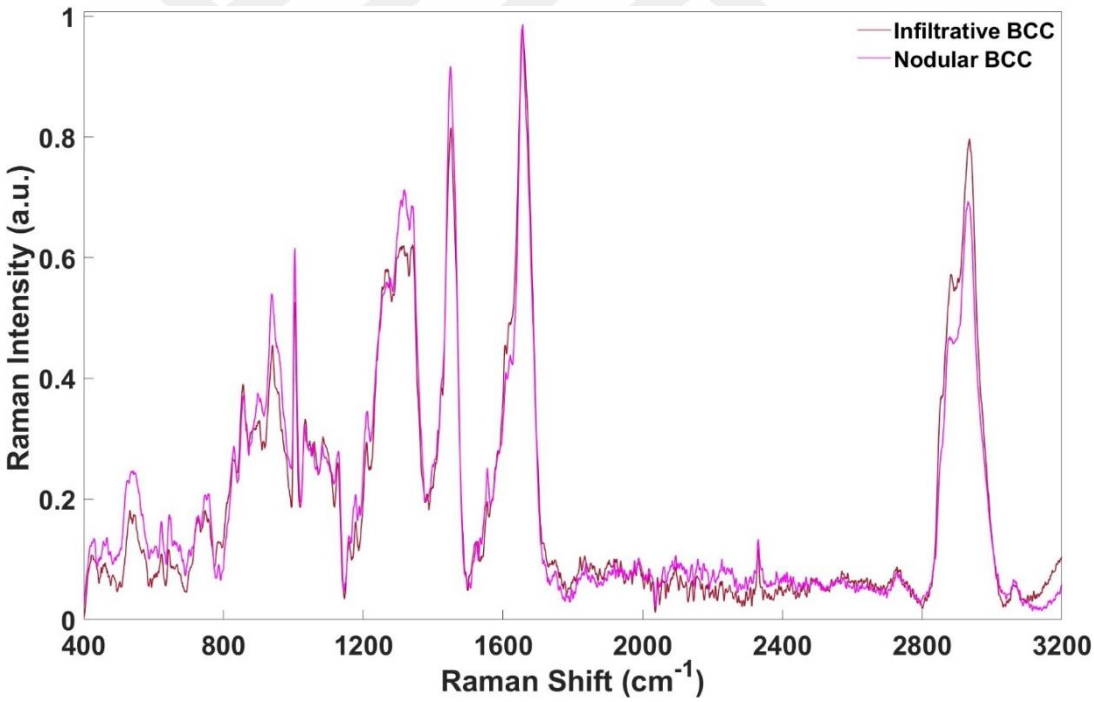

Figure 4.4 : Normalized mean Raman spectra of nodular BCC and infiltrative BCC tissues.

In the Figure 4.5, the average Raman spectra of nodular BCC (represented by a magenta solid line) and infiltrative BCC (represented by a burgundy solid line) skin tissues. Spectra are horizontally shifted for clarity. Vertical dashed lines denote the relative Raman shift peak positions between the spectra. Tables 4.5, 4.6, and 4.7 show the confusion matrices, performance metrics, and macro-averaged metrics for each supervised classifier, respectively.

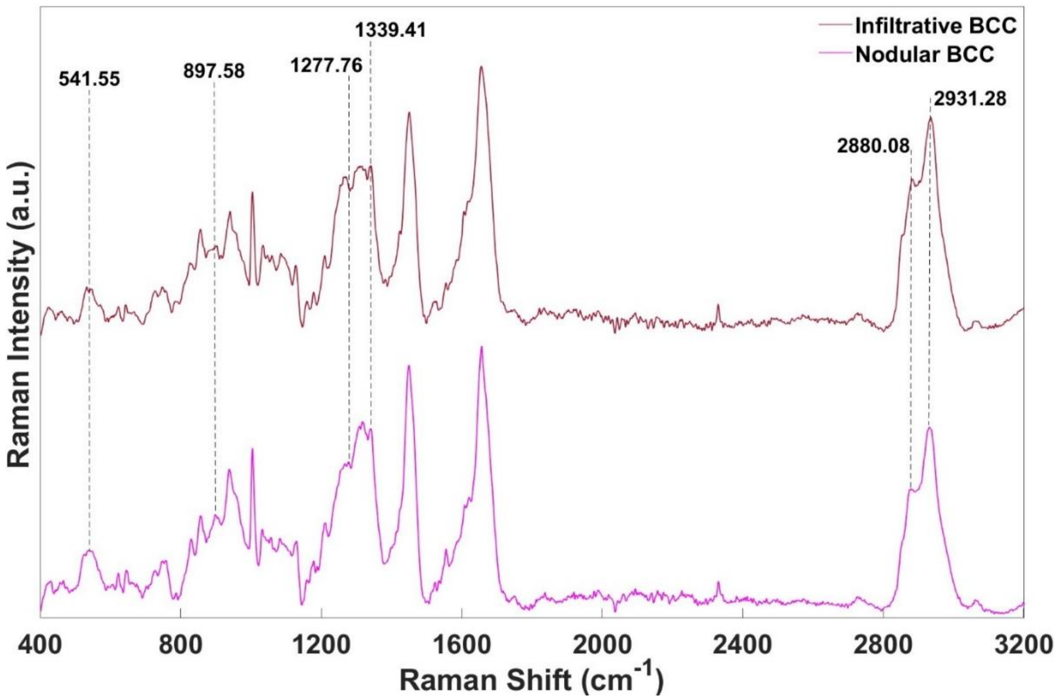

Figure 4.5 : Mean Raman spectra of nodular BCC and infiltrative BCC skin tissues.

Table 4.5 : Confusion matrices by each supervised classifier for nodular BCC and infiltrative BCC tissues.

Supervised Classification Models	Confusion Matrix		
	Classes	Nodular BCC	Infiltrative BCC
RF	Nodular BCC	523	47
	Infiltrative BCC	80	541
DT	Nodular BCC	526	82
	Infiltrative BCC	69	514
KNN (K=5)	Nodular BCC	536	68
	Infiltrative BCC	42	545
RF (with PCA, n = 3)	Nodular BCC	420	172
	Infiltrative BCC	167	432
LR	Nodular BCC	365	235
	Infiltrative BCC	194	397
LDA	Nodular BCC	376	255
	Infiltrative BCC	163	397
MLP (L = 8)	Nodular BCC	60	530
	Infiltrative BCC	54	547
SVM (C = 5)	Nodular BCC	410	195
	Infiltrative BCC	77	509
SVM (C = 100)	Nodular BCC	434	155
	Infiltrative BCC	68	534

Table 4.6 : Evaluation metrics of each supervised classifier for nodular BCC and infiltrative BCC tissues.

	Evaluation Metrics						
	Classes	Accuracy	Sensitivity	Specificity	PPV	NPV	F1 Score
RF	Nodular	0.893	0.872	0.917	0.92	0.867	0.895
	Infiltrative	0.893	0.92	0.867	0.871	0.917	0.895
DT	Nodular	0.873	0.882	0.865	0.862	0.884	0.872
	Infiltrative	0.873	0.862	0.884	0.881	0.865	0.871
KNN (K=5)	Nodular	0.907	0.928	0.887	0.889	0.927	0.908
	Infiltrative	0.907	0.889	0.927	0.928	0.887	0.908
RF (with PCA, n = 3)	Nodular	0.715	0.721	0.709	0.715	0.715	0.718
	Infiltrative	0.715	0.715	0.715	0.721	0.709	0.718
LR	Nodular	0.64	0.672	0.608	0.628	0.653	0.649
	Infiltrative	0.64	0.628	0.653	0.671	0.608	0.649
LDA	Nodular	0.65	0.789	0.595	0.609	0.697	0.655
	Infiltrative	0.65	0.608	0.697	0.708	0.595	0.655
MLP (L = 8)	Nodular	0.509	0.91	0.101	0.507	0.526	0.652
	Infiltrative	0.509	0.507	0.526	0.91	0.101	0.652
SVM (C = 5)	Nodular	0.772	0.868	0.677	0.723	0.842	0.789
	Infiltrative	0.772	0.723	0.868	0.868	0.723	0.789
SVM (C = 100)	Nodular	0.812	0.887	0.736	0.775	0.864	0.827
	Infiltrative	0.812	0.775	0.864	0.887	0.736	0.827

Table 4.7 : Macro-averaged metrics for each supervised classifier for nodular BCC and infiltrative BCC tissues.

	Macro-averaged Metrics					
	Accuracy	Sensitivity	Specificity	PPV	NPV	F1 Score
RF	0.893	0.896	0.892	0.895	0.892	0.895
DT	0.873	0.872	0.874	0.871	0.874	0.871
KNN (K=5)	0.907	0.908	0.907	0.908	0.907	0.908
RF (with PCA, n = 3)	0.715	0.718	0.712	0.718	0.712	0.718
LR	0.64	0.65	0.63	0.649	0.630	0.649
LDA	0.65	0.698	0.646	0.658	0.646	0.655
MLP (L = 8)	0.509	0.708	0.313	0.708	0.313	0.652
SVM (C = 5)	0.772	0.795	0.772	0.795	0.782	0.789
SVM (C = 100)	0.812	0.831	0.8	0.831	0.8	0.827

Although there is a marginal decline in precision when discerning between different subtypes of BCC in comparison to distinguishing BCC from normal skin, the study's method employing supervised ML classifiers maintained a notably high level of accuracy in discriminating nodular BCC from infiltrative BCC. According to the data presented in Table 4.6, the most exemplary performance was observed with RF and KNN classifiers, achieving accuracies of 89.3% and 90.7%, respectively, outperforming alternative models. Furthermore, the RF and KNN classifiers demonstrate sensitivity, specificity, PPV, NPV, and F1 scores all surpassing 87%, 86%, 87%, 86%, and 89%, respectively, across all evaluation criteria. As depicted in Table 4.7, the findings reveal that, in terms of macro-averaged metrics, the KNN classifier exhibits the most superior overall performance, attaining the highest macro-averaged accuracy of 90.7%. Nevertheless, it is evident that the MLP exhibits the least satisfactory performance, achieving an accuracy of 50.9%. This suboptimal performance may be attributed to the intricate architecture and abundance of parameters inherent in the MLP model, potentially leading to overfitting of the training dataset. Consequently, its ability to generalize to novel data is hindered [70]. The outcomes of this investigation underscore the potential of Raman spectroscopy in conjunction with ML as a robust and non-invasive technique for precise discrimination of BCC and its subtypes from normal skin tissues.

5. CONCLUSION AND FUTURE WORK

The present investigation presents a direct assessment of localized structural changes within the skin utilizing Raman spectroscopy. Leveraging Raman intensity and shift, the study facilitates the discrimination between BCC and normal skin, while also enabling the identification of BCC subtypes such as nodular and infiltrative. Notably, distinct variations in Raman peak intensities and shifts between BCC and normal skin, as well as between nodular and infiltrative types, are evident in the respective spectra. These discernible distinctions are attributed to molecular structural modifications within the skin induced by the presence of BCC. Following the preprocessing of raw data obtained from ex vivo fresh skin tissues, several supervised ML models were utilized to classify BCC from normal skin and distinguish between its various subtypes. The efficacy of each model was assessed using a diverse set of evaluation metrics. The findings reveal that RF and KNN classifiers exhibit exceptional accuracy of 98.4%, surpassing all other models for both BCC and normal tissues. Nonetheless, the KNN classifier achieved the most outstanding overall performance, boasting a macro-averaged accuracy of 90.7% for both nodular and infiltrative BCC. These results suggest that the integration of Raman spectroscopy with ML constitutes a potent and non-invasive approach for precisely distinguishing between BCC and normal skin, as well as identifying different subtypes of BCC. Future research activities could pursue various avenues to augment the potential and suitability of Raman spectroscopy in conjunction with ML for dermatological diagnostic purposes. First off, by capturing more complex molecular signatures connected to skin lesions, adding extra features taken from Raman spectra-like spectral shape parameters or higher-order statistical moments-may be able to enhance classification performance. Additionally, by automatically learning hierarchical representations of spectral data, integrating advanced ML techniques-like deep learning architectures like convolutional neural networks or recurrent neural networks-may offer enhanced discriminative power. These deep learning models may reveal subtle patterns in Raman spectra that are difficult to detect with conventional feature engineering techniques. They have shown impressive success in a variety of pattern recognition tasks. Furthermore, the establishment of a robust and uniform preprocessing pipeline for Raman spectral data could reduce the possibility of variability arising from data collection and processing, improving the repeatability and applicability of classification models in various experimental configurations and healthcare environments. A more thorough understanding of the discriminative ability of Raman spectroscopy for dermatological diagnostics would also be possible by expanding the research's scope to include a larger and more diverse dataset covering a wider range of skin conditions, such as benign lesions and other forms of skin cancer. It can be further leverage the synergistic potential of Raman spectroscopy and ML to transform the diagnosis and treatment of skin cancer and other dermatological conditions by pursuing these future research directions. This will ultimately advance personalized medicine and improve patient outcomes.

REFERENCES

[1] **Chmiel, P., Kłosińska, M., Forma, A., Pelc, Z., Gęca, K., & Skórzewska, M.** (2022). Novel approaches in non-melanoma skin cancers—a focus on hedgehog pathway in basal cell carcinoma (BCC). *Cells*, *11*(20), 3210.

[2] **Khayyati Kohnehshahri, M., Sarkesh, A., Mohamed Khosroshahi, L., HajiEsmailPoor, Z., Aghebati-Maleki, A., Yousefi, M., & Aghebati-Maleki, L.** (2023). Current status of skin cancers with a focus on immunology and immunotherapy. *Cancer Cell International*, *23*(1), 174.

[3] **Apalla, Z., Lallas, A., Sotiriou, E., Lazaridou, E., & Ioannides, D.** Epidemiological trends in skin cancer. Dermatology Practical & Conceptual. 2017; 7 (2): 1-6.

[4] **P. Santos, I., van Doorn, R., Caspers, P. J., Bakker Schut, T. C., Barroso, E. M., Nijsten, T. E., ... & Puppels, G. J.** (2018). Improving clinical diagnosis of early-stage cutaneous melanoma based on Raman spectroscopy. *British journal of cancer*, *119*(11), 1339-1346.

[5] **Xiang, F., Lucas, R., Hales, S., & Neale, R.** (2014). Incidence of nonmelanoma skin cancer in relation to ambient UV radiation in white populations, 1978-2012: empirical relationships. *JAMA dermatology*, *150*(10), 1063-1071.

[6] **P. Santos, I., van Doorn, R., Caspers, P. J., Bakker Schut, T. C., Barroso, E. M., Nijsten, T. E., ... & Puppels, G. J.** (2018). Improving clinical diagnosis of early-stage cutaneous melanoma based on Raman spectroscopy. *British journal of cancer*, *119*(11), 1339-1346.

[7] **Hasan, A., Kandil, A. M., Al-Ghamdi, H. S., Alghamdi, M. A., Nasr, M., Naeem, S. A., ... & Elgohary, S. A.** (2023). Sun-exposed versus sun-protected cutaneous basal cell carcinoma: clinico-pathological profile and p16 immunostaining. *Diagnostics*, *13*(7), 1271.

[8] **Neale, R. E., Davis, M., Pandeya, N., Whiteman, D. C., & Green, A. C.** (2007). Basal cell carcinoma on the trunk is associated with excessive sun exposure. *Journal of the American Academy of Dermatology*, *56*(3), 380-386.

[9] **Lear, J. T., & Smith, A. G.** (1997). Basal cell carcinoma. *Postgraduate medical journal*, *73*(863), 538-542.

[10] **Naik, P. P., & Desai, M. B.** (2022). Basal cell carcinoma: a narrative review on contemporary diagnosis and management. *Oncology and Therapy*, *10*(2), 317-335.

[11] **Bratchenko, I. A., Bratchenko, L. A., Khristoforova, Y. A., Moryatov, A. A., Kozlov, S. V., & Zakharov, V. P.** (2022). Classification of skin cancer using convolutional neural networks analysis of Raman spectra. *Computer Methods and Programs in Biomedicine, 219*, 106755.

[12] **Araújo, D. C., Veloso, A. A., de Oliveira Filho, R. S., Giraud, M. N., Raniero, L. J., Ferreira, L. M., & Bitar, R. A.** (2021). Finding reduced Raman spectroscopy fingerprint of skin samples for melanoma diagnosis through machine learning. *Artificial Intelligence in Medicine*, *120*, 102161.

[13] **Kuhar, N., Sil, S., Verma, T., & Umapathy, S.** (2018). Challenges in application of Raman spectroscopy to biology and materials. *RSC advances*, *8*(46), 25888-25908.

[14] **Ahmad, M. A., Eckert, C., & Teredesai, A.** (2018, August). Interpretable machine learning in healthcare. In *Proceedings of the 2018 ACM international conference on bioinformatics, computational biology, and health informatics* (pp. 559-560).

[15] **Butler, H. J., Ashton, L., Bird, B., Cinque, G., Curtis, K., Dorney, J., ... & Martin, F. L.** (2016). Using Raman spectroscopy to characterize biological materials. *Nature protocols*, *11*(4), 664-687.

[16]**Ahmed, B., Qadir, M. I., & Ghafoor, S.** (2020). Malignant melanoma: skin cancer− diagnosis, prevention, and treatment. *Critical Reviews™ in Eukaryotic Gene Expression*, *30*(4).

[17] **Vantuchova, Y., & Curik, R.** (2006). Histological types of basal cell carcinoma. *Scripta Medica (Brno)*, *79*(5-6), 261-70.

[18]**Schut, T. C. B., Caspers, P. J., Puppels, G. J., Nijssen, A., Heule, F., Neumann, M. H., & Hayes, D. P.** (2002). Discriminating basal cell carcinoma from its surrounding tissue by Raman spectroscopy. *Journal of investigative dermatology*, *119*(1), 64-69.

[19] **Reiter, O., Mimouni, I., Gdalevich, M., Marghoob, A. A., Levi, A., Hodak, E., & Leshem, Y. A.** (2019). The diagnostic accuracy of dermoscopy for basal cell carcinoma: a systematic review and meta-analysis. *Journal of the American Academy of Dermatology*, *80*(5), 1380-1388.

[20] **Haws, A. L., Rojano, R., Tahan, S. R., & Phung, T. L.** (2012). Accuracy of biopsy sampling for subtyping basal cell carcinoma. *Journal of the American Academy of Dermatology*, *66*(1), 106-111.

[21] **Kadouch, D. J., Leeflang, M. M., Elshot, Y. S., Longo, C., Ulrich, M., van der Wal, A. C., ... & de Rie, M. A.** (2017). Diagnostic accuracy of confocal microscopy imaging vs. punch biopsy for diagnosing and subtyping basal cell carcinoma. *Journal of the European Academy of Dermatology and Venereology*, *31*(10), 1641-1648.

[22] **Wang, L. F., Zhu, A. Q., Wang, Q., Li, X. L., Yan, J. N., Li, M. X., ... & Xu, H. X.** (2021). Value of high-frequency ultrasound for differentiating invasive basal cell carcinoma from non-invasive types. *Ultrasound in Medicine & Biology*, *47*(10), 2910-2920.

[23] **Hossam, D., Sadek, A., Wagih, A., & Malik, M.** (2015). Clinical photography of skin diseases. *Egyptian Dermatology Online Journal*, *369*(3245), 1-10.

[24] **Nijssen, A., Maquelin, K., Santos, L. F., Caspers, P. J., Bakker Schut, T. C., den Hollander, J. C., ... & Puppels, G. J.** (2007). Discriminating basal cell carcinoma from perilesional skin using high wave-number Raman spectroscopy. *Journal of biomedical optics*, *12*(3), 034004-034004.

[25] **Choi, J., Choo, J., Chung, H., Gweon, D. G., Park, J., Kim, H. J., ... & Oh, C. H.** (2005). Direct observation of spectral differences between normal and basal cell carcinoma (BCC) tissues using confocal Raman microscopy. *Biopolymers: Original Research on Biomolecules*, *77*(5), 264-272.

[26] **Silveira Jr, L., Silveira, F. L., Bodanese, B., Zângaro, R. A., & Pacheco, M. T. T.** (2012). Discriminating model for diagnosis of basal cell carcinoma and melanoma in vitro based on the Raman spectra of selected biochemicals. *Journal of biomedical optics*, *17*(7), 077003-077003.

[27] **Das, K., Cockerell, C. J., Patil, A., Pietkiewicz, P., Giulini, M., Grabbe, S., & Goldust, M.** (2021). Machine learning and its application in skin cancer. *International Journal of Environmental Research and Public Health*, *18*(24), 13409.

[28] **Mo, H., Wang, E., Tian, Y., Pu, Y., Wu, B., & Alfano, R. R.** (2021, March). Analysis of Stokes shift spectra for distinguishing human prostate cancerous and normal tissues using machine learning methods. In *Photonic Diagnosis, Monitoring, Prevention, and Treatment of Infections and Inflammatory Diseases 2021* (Vol. 11626, pp. 47-54). SPIE.

[29] **Widjaja, E., Zheng, W., & Huang, Z.** (2008). Classification of colonic tissues using near-infrared Raman spectroscopy and support vector machines. *International journal of oncology*, *32*(3), 653-662.

[30] **Krafft, C., Steiner, G., Beleites, C., & Salzer, R.** (2009). Disease recognition by infrared and Raman spectroscopy. *Journal of biophotonics*, *2*(1-2), 13-28.

[31] **Campanella, G., Navarrete-Dechent, C., Liopyris, K., Monnier, J., Aleissa, S., Minhas, B., ... & Jain, M.** (2022). Deep learning for basal cell carcinoma detection for reflectance confocal microscopy. *Journal of Investigative Dermatology*, *142*(1), 97-103.

[32] **Niazi, A., Parvin, P., Jafargholi, A., Basam, M. A., Khodabakhshi, Z., Bavali, A., ... & Moafi, A.** (2022). Discrimination of normal and cancerous human skin tissues based on laser-induced spectral shift fluorescence microscopy. *Scientific Reports*, *12*(1), 20927.

[33] **Serzhantov, K. A., Myakinin, O. O., Lisovskaya, M. G., Bratchenko, I. A., Moryatov, A. A., Kozlov, S. V., & Zakharov, V. P.** (2020, April). Comparison testing of machine learning algorithms separability on Raman spectra of skin cancer. In *Biomedical Spectroscopy, Microscopy, and Imaging* (Vol. 11359, pp. 32-38). SPIE.

[34] **Matousek, P., & Stone, N.** (2013). Recent advances in the development of Raman spectroscopy for deep non-invasive medical diagnosis. *Journal of biophotonics*, *6*(1), 7-19.

[35] **Smith, E., & Dent, G.** (2019). *Modern Raman spectroscopy: a practical approach*. John Wiley & Sons.

[36] **Movasaghi, Z., Rehman, S., & Rehman, I. U.** (2007). Raman spectroscopy of biological tissues. *Applied Spectroscopy Reviews*, *42*(5), 493-541.

[37] **Xu, Z., He, Z., Song, Y., Fu, X., Rommel, M., Luo, X., ... & Fang, F.** (2018). Topic review: application of Raman spectroscopy characterization in micro/nano-machining. *Micromachines*, *9*(7), 361.

[38] **Ntziouni, A., Thomson, J., Xiarchos, I., Li, X., Bañares, M. A., Charitidis, C., ... & Diz, E. L.** (2022). Review of Existing Standards, Guides, and Practices for Raman Spectroscopy. *Applied Spectroscopy*, *76*(7), 747-772.

[39] **Press, W. H., & Teukolsky, S. A.** (1990). Savitzky-Golay smoothing filters. *Computers in Physics*, *4*(6), 669-672.

[40] **Sen, P. C., Hajra, M., & Ghosh, M.** (2020). Supervised classification algorithms in machine learning: A survey and review. In *Emerging Technology in Modelling and Graphics: Proceedings of IEM Graph 2018* (pp. 99-111). Springer Singapore.

[41] **Dhall, D., Kaur, R., & Juneja, M.** (2020). Machine learning: a review of the algorithms and its applications. *Proceedings of ICRIC 2019: Recent innovations in computing*, 47-63.

[42] **Jabbar, H., & Khan, R. Z.** (2015). Methods to avoid over-fitting and under-fitting in supervised machine learning (comparative study). *Computer Science, Communication and Instrumentation Devices*, *70*(10.3850), 978-981.

[43] **Amjad, A., Ullah, R., Khan, S., Bilal, M., & Khan, A.** (2018). Raman spectroscopy based analysis of milk using random forest classification. *Vibrational Spectroscopy*, *99*, 124-129.

[44] **Yuan, Y., Wu, L., & Zhang, X.** (2021). Gini-impurity index analysis. *IEEE Transactions on Information Forensics and Security*, *16*, 3154-3169.

[45] **Navada, A., Ansari, A. N., Patil, S., & Sonkamble, B. A.** (2011, June). Overview of use of decision tree algorithms in machine learning. In *2011 IEEE control and system graduate research colloquium* (pp. 37-42). IEEE.

[46] **Tangirala, S.** (2020). Evaluating the impact of GINI index and information gain on classification using decision tree classifier algorithm. *International Journal of Advanced Computer Science and Applications*, *11*(2), 612-619.

[47] **Taunk, K., De, S., Verma, S., & Swetapadma, A.** (2019, May). A brief review of nearest neighbor algorithm for learning and classification. In *2019 international conference on intelligent computing and control systems (ICCS)* (pp. 1255-1260). IEEE.

[48] **Zhang, S., Li, X., Zong, M., Zhu, X., & Cheng, D.** (2017). Learning k for knn classification. *ACM Transactions on Intelligent Systems and Technology (TIST)*, *8*(3), 1-19.

[49] **Boateng, E. Y., & Abaye, D. A.** (2019). A review of the logistic regression model with emphasis on medical research. *Journal of data analysis and information processing*, *7*(04), 190.

[50] **Domínguez-Almendros, S., Benítez-Parejo, N., & Gonzalez-Ramirez, A. R.** (2011). Logistic regression models. *Allergologia et immunopathologia*, *39*(5), 295-305.

[51] **Balakrishnama, S., & Ganapathiraju, A.** (1998). Linear discriminant analysis-a brief tutorial. *Institute for Signal and information Processing*, *18*(1998), 1-8.

[52] **Abraham, A.** (2005). Artificial neural networks. *Handbook of measuring system design*.

[53] **Pisner, D. A., & Schnyer, D. M.** (2020). Support vector machine. In *Machine learning* (pp. 101-121). Academic Press.

[54] **Lui, H., Zhao, J., McLean, D., & Zeng, H.** (2012). Real-time Raman spectroscopy for in vivo skin cancer diagnosis. *Cancer research*, *72*(10), 2491-2500.

[55**] Santos, I. P., Caspers, P. J., Bakker Schut, T. C., van Doorn, R., Noordhoek Hegt, V., Koljenović, S., & Puppels, G. J.** (2016). Raman spectroscopic characterization of melanoma and benign melanocytic lesions suspected of melanoma using high-wavenumber Raman spectroscopy. *Analytical chemistry*, *88*(15), 7683-7688.

[56] **Silveira, F. L., Pacheco, M. T., Bodanese, B., Pasqualucci, C. A., Zângaro, R. A., & Silveira Jr, L.** (2015). Discrimination of non-melanoma skin lesions from non-tumor human skin tissues in vivo using Raman spectroscopy and multivariate statistics. *Lasers in surgery and medicine*, *47*(1), 6-16.

[57] **Lunter, D., Klang, V., Kocsis, D., Varga-Medveczky, Z., Berkó, S., & Erdő, F.** (2022). Novel aspects of Raman spectroscopy in skin research. *Experimental Dermatology*, *31*(9), 1311-1329.

[58] **Lima, A. M. F., Daniel, C. R., Navarro, R. S., Bodanese, B., Pasqualucci, C. A., Pacheco, M. T. T., ... & Silveira Jr, L.** (2019). Discrimination of non-melanoma skin cancer and keratosis from normal skin tissue in vivo and ex vivo by Raman spectroscopy. *Vibrational Spectroscopy*, *100*, 131-141.

[59] **Gąsior-Głogowska, M., Komorowska, M., Hanuza, J., Mączka, M., Zając, A., Ptak, M., ... & Szotek, S.** (2013). FT-Raman spectroscopic study of human skin subjected to uniaxial stress. *Journal of the mechanical behavior of biomedical materials*, *18*, 240-252.

[60] **Mogensen, M., & Jemec, G. B.** (2007). Diagnosis of nonmelanoma skin cancer/keratinocyte carcinoma: a review of diagnostic accuracy of nonmelanoma skin cancer diagnostic tests and technologies. *Dermatologic Surgery*, *33*(10), 1158-1174.

[61] **Pezzotti, G., Boffelli, M., Miyamori, D., Uemura, T., Marunaka, Y., Zhu, W., & Ikegaya, H.** (2015). Raman spectroscopy of human skin: looking for a quantitative algorithm to reliably estimate human age. *Journal of Biomedical Optics*, *20*(6), 065008-065008.

[62] **Lunter, D., Klang, V., Kocsis, D., Varga-Medveczky, Z., Berkó, S., & Erdő, F.** (2022). Novel aspects of Raman spectroscopy in skin research. *Experimental Dermatology*, *31*(9), 1311-1329.

[63] **Silveira Jr, L., Silveira, F. L., Bodanese, B., Zângaro, R. A., & Pacheco, M. T. T.** (2012). Discriminating model for diagnosis of basal cell carcinoma and melanoma in vitro based on the Raman spectra of selected biochemicals. *Journal of biomedical optics*, *17*(7), 077003-077003.

[64] **Feng, X., Fox, M. C., Reichenberg, J. S., Lopes, F. C., Sebastian, K. R., Markey, M. K., & Tunnell, J. W.** (2019). Biophysical basis of skin cancer margin assessment using Raman spectroscopy. *Biomedical optics express*, *10*(1), 104-118.

[65] **Feng, X., Moy, A. J., Nguyen, H. T., Zhang, J., Fox, M. C., Sebastian, K. R., ... & Tunnell, J. W.** (2017). Raman active components of skin cancer. *Biomedical optics express*, *8*(6), 2835-2850.

[66] **Movasaghi, Z., Rehman, S., & Rehman, I. U.** (2007). Raman spectroscopy of biological tissues. *Applied Spectroscopy Reviews*, *42*(5), 493-541.

[67] **Ali, S. M., Bonnier, F., Tfayli, A., Lambkin, H., Flynn, K., McDonagh, V., ... & Byrne, H. J.** (2013). Raman spectroscopic analysis of human skin tissue sections ex-vivo: evaluation of the effects of tissue processing and dewaxing. *Journal of Biomedical Optics*, *18*(6), 061202-061202.

[68] **Martinez, M. G., Bullock, A. J., MacNeil, S., & Rehman, I. U.** (2019). Characterisation of structural changes in collagen with Raman spectroscopy. *Applied Spectroscopy Reviews*, *54*(6), 509-542.

[69] **Niculet, E., Craescu, M., Rebegea, L., Bobeica, C., Nastase, F., Lupasteanu, G., ... & Tatu, A. L.** (2022). Basal cell carcinoma: Comprehensive clinical and histopathological aspects, novel imaging tools and therapeutic approaches. *Experimental and therapeutic medicine*, *23*(1), 1-8.

[70] **Rynkiewicz, J.** (2012). General bound of overfitting for MLP regression models. *Neurocomputing*, *90*, 106-110.

CURRICULUM VITAE

Name SURNAME **:** Muhammet Melih GÜLER

EDUCATION **:**

- **B.Sc.** **:** 2021, Istanbul Technical University, Electrical & Electronics Faculty, Control & Automation Engineering

PROFESSIONAL EXPERIENCE AND REWARDS:

- 2021-Present, Software Engineer

PUBLICATIONS, PRESENTATIONS AND PATENTS ON THE THESIS:

- **Güler, M.**, Kurt, O., Baş, S., Özkesici Kurt, B., Kırgöz, H., Nar, I., Hasçiçek, S. Ö., & Altınel, D. (2024). Enhancing skin cancer diagnosis through the integration of Raman spectroscopy and machine learning. In Ş. Filiz & H. Andıç (Eds.), *Proceedings of the 5th International Mediterranean Scientific Research and Innovation Congress* (pp. 492-499). ISARC International Science and Art Research Center.